J. Physiol. (1987), **383**, *pp.* 653–692
With 17 text-figures and 1 plate
Printed in Great Britain

PASSIVE CABLE PROPERTIES AND MORPHOLOGICAL CORRELATES OF NEURONES IN THE LATERAL GENICULATE NUCLEUS OF THE CAT

BY STEWART A. BLOOMFIELD, JAMES E. HAMOS AND S. MURRAY SHERMAN

From the Department of Neurobiology and Behavior, State University of New York, Stony Brook, NY 11794, U.S.A.

(*Received 15 November 1985*)

SUMMARY

1. We used an *in vivo* preparation of the cat to study the passive cable properties of sixteen X and twelve Y cells in the lateral geniculate nucleus. Cells were modelled as equivalent cylinders according to Rall's formulations (Rall, 1959*a*, 1969, 1977). We injected intracellular current pulses into these geniculate neurones, and we analysed the resulting voltage transients to obtain the cable parameters of these cells. In addition, fifty-four physiologically characterized neurones were labelled with horseradish peroxidase (HRP) and analysed morphologically.

2. Analysis of HRP-labelled geniculate neurones showed that the dendritic branching pattern of these cells adheres closely to the $\frac{3}{2}$ power rule. That is, at each branch point, the diameter of the parent branch raised to the $\frac{3}{2}$ power equals the sum of the diameters of the daughter dendrites after each is raised to the $\frac{3}{2}$ power. Furthermore, preliminary data indicate that the dendritic terminations emanating from each primary dendrite occur at the same electrotonic distance from the soma. These observations suggest that both X and Y cells meet the geometric constraints necessary for reduction of their dendritic arbors into equivalent cylinders.

3. We found a strong linear relationship between the diameter of each primary dendrite and the membrane surface area of the arbor emanating from it. We used this relationship to derive an algorithm for determining the total somatic and dendritic membrane surface area of an X or Y cell simply from knowledge of the diameters of its soma and primary dendrites.

4. Both geniculate X and Y cells display current–voltage relationships that were linear within ± 20 mV of the resting membrane potential. This meant that we could easily remain within the linear voltage range during the voltage transient analyses.

5. X and Y cells clearly differ in terms of many of their electrical properties, including input resistance, membrane time constant and electrotonic length. The difference in input resistance between X and Y cells cannot be attributed solely to the smaller average size of X cells, but it also reflects a higher specific membrane resistance (R_m) of the X cells. Furthermore, X cells exhibit electrotonic lengths slightly larger than those of Y cells, but both neuronal types display electrotonic lengths of roughly 1. This indicates that even the most distally located innervation to these cells should have considerable influence on their somatic and axonal responses.

6. The relationship between membrane time constant and electrotonic length suggests that the Y cell population has rather uniform dendritic geometry (i.e. they are scaled in size) whereas X cells are more variable in terms of their dendritic geometry. This finding agrees with morphological data reported here and by others (Friedlander, Lin, Stanford & Sherman, 1981).

7. We utilized an expression derived from the equivalent cylinder model to calculate the specific membrane capacitance (C_m) for eight neurones that were studied biophysically and subsequently labelled with HRP. Both X and Y cells display similar values for C_m, with a mean for the eight neurones of 1·86 μF/cm^2. With the assumption of a constant C_m for all geniculate cells, the R_m values of all twenty-eight geniculate neurones were calculated from measurements of the membrane time constants. X cells show higher R_m values than do Y cells. In addition, X cells showed considerable heterogeneity in their values for R_m, whereas values for R_m are rather constant across the Y cell population.

8. The present results suggest that the cable parameters of geniculate neurones over-all are not simply correlated to cell size. This is largely due to X cells having greater and more variable values for R_m than do Y cells. Within the Y cell class, the electrical properties appear to correlate fairly well to cell size, whereas the electrical parameters of X cells cannot be explained by any simple factor of size scaling. X cell electrical parameters seem to reflect variations in specific R_m and variations in dendritic geometry.

9. The relatively high values of R_m for X cells serve to reduce their electrotonic length. This, in turn, may compensate for the relative thinness of X cell dendrites compared to those of Y cells. Furthermore, the variability in the values of R_m for X cells may offset variability in the dendritic geometry of these cells, thereby ensuring uniform values of electrotonic length across the X cell population.

INTRODUCTION

In the cat, the pathway from the retina through laminae A and A1 of the lateral geniculate nucleus to the visual cortex is comprised of two parallel, independent neuronal streams known as the X and Y cell pathways (Stone, Dreher & Leventhal, 1979; Lennie, 1980; Sherman & Spear, 1982; Sherman, 1985). In the context of this organization, the lateral geniculate nucleus has been generally regarded as a mere relay whose function is the transfer of visual information from retina to cortex without significant elaboration of receptive field properties. This idea has stemmed from the fact that geniculate X and Y cells receive their retinal inputs from one or a few ganglion cells of the same X or Y cell class and of the same on- or off-centre receptive field type (Cleland, Dubin & Levick, 1971; Hoffmann, Stone & Sherman, 1972). The receptive field properties of geniculate cells are thus virtually identical to those of their retinal afferent inputs (Hubel & Wiesel, 1961; Kaplan, Marcus & So, 1979; So & Shapley, 1981). However, only 10–20 % of the synapses on geniculate relay cells are retinal in origin (Guillery, 1969*a*, *b*; Wilson, Friedlander & Sherman, 1984), and activation of many non-retinal inputs (e.g. from the mid-brain and pons) dramatically alters the excitability of these cells (Singer, 1973; Foote, Mordes, Colby & Harrison, 1977; Ahlsén, Lindström & Lo, 1984). It is thus abundantly clear that

geniculate cells integrate information from many non-retinal excitatory and inhibitory inputs, and it has been suggested that the lateral geniculate nucleus may serve to gate or control the gain of signal transmission from retina to cortex (Singer, 1977; Crick, 1984; Sherman & Koch, 1986).

To understand the integrative performance of geniculate neurones, several anatomical studies have been initiated to study the pattern of afferent inputs to these cells (Guillery, 1969*a*, *b*; Wilson *et al.* 1984; Hamos, Van Horn, Raczkowski & Sherman, 1986). However, one must also have a description of their passive electrical or cable properties, because these parameters play a crucial role in determining synaptic current flow within a neurone's dendritic tree. The passive cable properties of dendrites, in conjunction with synaptic location, largely determine the amplitude and duration of post-synaptic potentials recorded at the soma (for reviews, see Rall, 1959*b*, 1970, 1977; Jack, Noble & Tsien, 1975).

Due largely to technical considerations, studies of neuronal cable properties in the mammalian central nervous system have focused mostly on *in vivo* preparations of the relatively large spinal motoneurones (Nelson & Lux, 1970; Burke & ten Bruggencate, 1971; Iansek & Redman, 1973; Barrett & Crill, 1974; for a review, see Rall, 1977) or on *in vitro* preparations, such as brain slices, that may disrupt the morphological relationships of the neurones under study and severely limit the opportunity to stimulate these neurones via their natural afferent pathways. Furthermore, many of these latter studies have been directed at neuronal populations, such as hippocampal cells (Turner & Schwartzkroin, 1980; Brown, Fricke & Perkel, 1981*a*; Durand, Carlen, Gurevich, Ho & Kunov, 1983), for which knowledge of basic functional roles and/or morphological patterns of identified synaptic inputs is lacking.

In contrast to this, the cat's lateral geniculate nucleus offers two major advantages not generally found elsewhere in the mammalian central nervous system for the study of cable properties. First, as noted above, the functionally distinct X and Y cell classes coexist in geniculate laminae A and A1. We can thus determine with the same techniques and preparations the extent to which these two neuronal types possess different passive electrical properties and, moreover, what contribution the cable properties might make to the different responses of these X and Y cells. Secondly, it is of obvious interest to relate the cable properties of these neurones to their distinctive morphological features. In particular, geniculate X cells possess somatic and dendritic morphology plus a pattern of synaptic inputs that differ from those of Y cells (Friedlander *et al.* 1981; Wilson *et al.* 1984; Hamos *et al.* 1986). Consequently, a biophysical analysis of the cable properties of geniculate neurones not only provides a more complete description of these cells, but it affords a unique opportunity to relate these parameters to other well-documented anatomical and functional features of these cells.

In the present study, we have investigated the passive cable properties of geniculate neurones from an *in vivo* preparation of the cat by modelling these neurones as equivalent cylinders (Rall, 1959*a*, 1977). In addition, by combining intracellular recording and labelling of some cells with horseradish peroxidase (HRP), we have been able to determine both the cable properties of identified X or Y cells as well as their somatic and dendritic morphological properties.

Our results indicate that geniculate X and Y cells are electrically quite compact (i.e. their electrotonic lengths are roughly 1), which implies that even the most distal innervation on their dendritic arbors may have considerable influence on their somatic and axonal responses. Furthermore, certain of the cable properties of X cells differ from those of Y cells. Some of these differences are not simply reflexions of the smaller anatomical size of X cells relative to that of Y cells, but instead seem to reflect variability between the physiological classes in terms of their intrinsic membrane structure.

Portions of these data have been presented in preliminary form elsewhere (Bloomfield & Sherman, 1984; Bloomfield, Hamos & Sherman, 1985).

METHODS

General preparation

Many of the general methods used during these experiments have been described previously (Friedlander *et al.* 1981; Stanford, Friedlander & Sherman, 1983; Sur & Sherman, 1982; Humphrey, Sur, Uhlrich & Sherman, 1985), and a brief summary follows. We initially anaesthetized normal adult cats (2·0–3·5 kg) with 4 % halothane delivered in a 50/50 mixture of nitrous oxide and oxygen, cannulated the femoral vein to allow the infusion of paralytic agents plus supplemental doses of barbiturate, and performed a tracheotomy to insert an endotracheal tube. We placed the animal in a stereotaxic device and changed the level of anaesthetic for all subsequent surgery to 1 % halothane in a 70/30 mixture of nitrous oxide and oxygen. The cat was paralysed with a 5 mg bolus of gallamine triethiodide followed by a continuous infusion of 3·6 mg gallamine triethiodide/h, 0·7 mg *d*-tubocurarine/h, and 6 ml 5 % lactated Ringer solution/h. We then artificially respired the animal and kept its end-tidal carbon dioxide at a level of 4 %. We made small craniotomies and durotomies to introduce the stimulating and recording electrodes into the brain. These openings were hydraulically sealed during recording. Following surgery, all wounds and pressure points were infiltrated at regular intervals with 1 % lidocaine. We then discontinued halothane and maintained the animal for the remaining 24–36 h of the experiment on a 70/30 mixture of nitrous oxide and oxygen plus sodium pentobarbitone administered at a rate of 1 mg/h for each kilogram of body weight. Body temperature was maintained at 37 °C with a thermostatically controlled heating blanket. In addition, heart rate and e.e.g. (electroencephalogram) were monitored throughout the course of an experiment.

Visual stimulation

Atropine sulphate and phenylephrine were topically applied to the cats' eyes to dilate the pupils and retract the nictitating membranes. We then fitted the corneas with contact lenses chosen by retinoscopy to ensure that each retina was focused on the targets used for visual stimulation. We projected the optic disk of each eye onto a frontal tangent screen by the method of Fernald & Chase (1971). Neuronal receptive field positions were measured with respect to that of the optic disk and, in turn, to that of the area centralis (e.g. Sanderson & Sherman, 1971). By using Sanderson's (1971) maps of the lateral geniculate nucleus, we could confidently match the histological location of each HRP-labelled neurone with the appropriate receptive field location.

Responses to spatial sine-wave gratings, either sinusoidally or rectilinearly modulated in time, were used to determine the spatial and temporal summation properties of cells. The gratings were generated on a cathode ray tube with spatial frequency, temporal frequency, and spatial phase continuously variable. The gratings had a mean luminance of 40 cd/m^2 and a contrast that could be continuously varied up to 0·6; for most measures, we employed a contrast of 0·6. Neuronal responses to the gratings were Fourier analysed in order to assess the linearity of these responses (Hochstein & Shapley, 1976; Shapley & Lennie, 1985). Cells were considered to sum linearly if their responses were generated primarily at the fundamental temporal frequency of the stimulus and showed sinusoidal spatial phase dependency, with practically no modulated response at one spatial phase (the null position) and a maximal response to a phase angle of 90 deg from the null position. Cells with non-linear summation displayed significant response components at twice the temporal

frequency of the stimulus, and these doubling responses were essentially independent of the spatial phase of the stimulus.

Electrophysiological recordings

We fashioned recording electrodes from omega-dot glass tubing (outer diameter of 1·2 mm, inner diameter of 0·7 mm) on a vertical puller. We filled each pipette with one of three solutions: (1) 4 M-potassium chloride, (2) 4 M-potassium acetate, or (3) 5 % HRP (Sigma VI) plus 0·2 M-potassium chloride in 0·05 M-Tris buffer. We then bevelled each micropipette to a final impedance (measured at 100 Hz) of 20–60 MΩ for electrodes filled with potassium chloride or potassium acetate and 65–110 MΩ for electrodes filled with HRP. Recordings were made using a high-impedence amplifier equipped with a bridge and current injection circuitry. We used a hydraulic microdrive to advance the electrodes to the lateral geniculate nucleus. All but one of the geniculate cells included in this paper were recorded in laminae A and A1; the exception was a Y cell located in lamina C.

Bipolar stimulating electrodes were inserted across the optic chiasm to effect orthodromic activation of geniculate neurones. The latency of activation from the stimulation site was measured as the time from the stimulus artifact to the foot of the action potential or excitatory post-synaptic potential. In half of the experiments, an array of four stimulating electrodes was placed in the cortical grey matter of areas 17 and 18 and pairs were used for bipolar stimulation to elicit antidromic activation of geniculate cells. Such activation was verified by triggering the cortical stimulus from a spontaneous orthodromic action potential in the geniculate cell. This ensured that the orthodromic spike collided with and cancelled the antidromic spike, preventing the latter from invading the soma.

We studied several response properties of each geniculate neurone prior to biophysical analysis. These included response latency to electrical stimulation of the optic chiasm (and of cortex for those animals in which cortical electrodes were used), ocular dominance, receptive field position, centre size, centre–surround properties, responses to the modulated sine-wave gratings, responses to standing contrasts, and responses to fast-moving targets. From these responses, we identified geniculate neurones as X or Y cells (see Stone *et al.* 1979; Lennie, 1980; Sherman & Spear, 1982; Sherman, 1985; Shapley & Lennie, 1985).

Approximately one-half of the neurones were identified as X or Y cells during extracellular recordings. We then slowly advanced the electrode until we observed fluctuations in the recorded potential. Cells were then impaled either by applying brief (50 ms) positive current pulses of 2–10 nA through the recording micropipette, by oscillating the amplifier through over-adjustment of the capacitance compensation circuit, or by physically tapping the micro-electrode holder. Intracellular impalement was indicated by a large, d.c. drop in recorded potential, the appearance of post-synaptic potentials, and large, positive action potentials. Immediately after impalement of a neurone, we quickly re-analysed its response properties to ensure that the impaled cell was the same one that we studied extracellularly. The remaining half of the cells in our study were impaled immediately and thus analysed solely during intracellular recording.

For those cells studied with HRP-filled electrodes, physiological analysis was first performed, and then HRP was ionophoresed into the neurone with 50–100 ms positive current pulses of 3–10 nA at 5 Hz for 2–20 min. The activity of the neurone was monitored intermittently to ensure that the electrode was still inside the same cell. Following HRP ionophoresis, we withdrew the electrode from the brain and repositioned it at least 500 μm distant to any other penetration.

Biophysical measurements

We took precautions to minimize artifacts introduced into our data by the recording system, particularly since biophysical properties were measured with a single-electrode recording paradigm requiring a bridge circuit. We collected data only from electrodes that, with optimum capacitance compensation, displayed time-to-peak responses of 300 μs or less to a square-wave current pulse when measured at the level of the lateral geniculate nucleus; this corresponded to time constants of 100–250 μs. During several of the experiments we utilized a driven shield to reduce electrode capacitance to acceptable levels. We also required that each electrode show no sign of rectification when currents of up to 5 nA were delivered across its tip. As soon as any change in the recording characteristics of an electrode was detected during a penetration, the recording was immediately terminated. When electrode characteristics changed appreciably, any data collected after the electrode was last verified to have behaved stably were discarded.

We adopted minimum requirements for acceptable intracellular recording. These included a stable resting membrane potential (V_m) of at least -50 mV (with a mean for the acceptable neurones of -60 mV), a spike amplitude of at least 30 mV (with a mean of 39 mV), and clear activation of synaptic potentials by stimulation of the optic chiasm. We used the bridge to balance or cancel the extracellular resistance (corresponding to the resistance of the electrode and recording system) and then determined the input resistance (R_n) of each neurone by measuring the voltage response to depolarizing and hyperpolarizing constant current pulses with amplitudes of 0·25 nA and durations of 250–500 ms. We also measured current–voltage (I–V) relationships of several neurones with similar current pulses ranging in amplitude up to 2·0 nA.

We modelled each geniculate neurone as an equivalent cylinder with a lumped somatic impedance at one end and a closed terminus at the other (Rall, 1959*a*, 1969, 1977). We determined the membrane time constant (τ_m) of each cell via the method of exponential peeling of the transient voltage response to a hyperpolarizing constant current step (Rall, 1969). The hyperpolarizing current steps were 50 ms in duration and 0·25–0·50 nA in amplitude. Voltage responses to each of these current steps were sampled at a rate of 7 kHz and averaged for 100–200 trials by computer. We also analysed four of the cells with current pulses lasting only 0·5 ms (Jack & Redman, 1971; Iansek & Redman, 1973; Durand *et al.* 1983). Unfortunately, the rather high current amplitudes (5–10 nA) required with the 0·5 ms pulses often caused rectification of our electrodes, prompting us to abandon this technique.

The charging response of a neurone to an injection of constant current is the sum of exponentials (Rall, 1969):

$$V_f - V = C_0 e^{-t/\tau_0} + C_1 e^{-t/\tau_1} + C_2 e^{-t/\tau_2} + \ldots, \quad (1)$$

where V is the initial resting membrane potential, V_f is the final, steady-state resting potential, the C_i values are coefficients that depend on the initial distribution of membrane polarization and the point of observation, t is time after start of current injection, τ_0 is the membrane time constant, and the τ_i values are the equalizing time constants. The natural logarithm of the voltage was plotted against time and the resulting curve was then 'peeled' by a computer-driven algorithm to derive the time constants and coefficients. In practice, only the longest time constant ($\tau_0 = \tau_m$) and the two longest equalizing time constants (τ_1 and τ_2) could be clearly resolved.

We used the first two time constants to calculate the electrotonic length of the entire neurone (L_n), including the soma, from Rall's (1969) formulations:

$$\alpha = [(\tau_0/\tau_1) - 1]^{\frac{1}{2}}, \quad (2)$$

$$L_n = \pi/\alpha. \quad (3)$$

The ratio of the dendritic-to-somatic conductance (ρ) was estimated from the relationship reported by Brown, Perkel, Norris & Peacock (1981*b*):

$$\rho = (\tau_0/V_f)[(C_0/\tau_0) + (C_1/\tau_1)] - 1. \quad (4)$$

The electrotonic length (L) of the uniform cylinder most equivalent to the dendritic tree may then be approximated by:

$$L = \pi[\rho/(\rho+1)]/(\tau_0/\tau_1 - 1)^{\frac{1}{2}}. \quad (5)$$

We employed this estimate for L as a starting point to obtain its more accurate value by computer iteration of the transcendental equation (Rall, 1969):

$$\rho + [\alpha \cot(\alpha L) \tanh(L)] = 0. \quad (6)$$

When a neurone consists of dendrites that can be reduced to equivalent cylinders of equal L (this criterion is satisfied by geniculate neurones; see Results), R_m can be derived by the equation (Rall, 1977):

$$R_m = [A_n R_n \tanh(L_n)]/L_n, \quad (7)$$

where A_n is the total membrane surface area of the cell's soma and dendrites. Several geniculate neurones for which we determined R_n and L_n were labelled with HRP, as described above, and A_n calculated. For these cells, we could then estimate R_m using eqn. (7). Finally, we could estimate C_m from:

$$C_m = \tau_m/R_m. \quad (8)$$

Histology

Light microscopy. Cats in which HRP labelling of geniculate neurones was performed were sacrificed at least 1 h after the final HRP injection with a lethal dose of pentobarbitone. We then transcardially perfused them with a 2 l mixture of 1 % paraformaldehyde and 2 % gluteraldehyde in 0·1 M-phosphate buffer (pH 7·4) followed by a 1 l rinse of 10 % sucrose in phosphate buffer. The brain was blocked stereotaxically and placed in 30 % sucrose solution overnight. Serial coronal sections were cut on a freezing microtome at a thickness of 100 μm. These sections were reacted with diaminobenzidine, and the reaction was intensified with cobaltous chloride (Adams, 1977).

We reconstructed cells at roughly 1000 × by using a drawing-tube attachment on a light microscope fitted with a 100 × oil-immersion objective (N.A. 1·32). We measured morphological features (soma sizes and dendritic diameters) directly under the microscope by using the same optics with an eyepiece graticule. We assume a resolution of 0·5 μm for these measurements (Friedlander *et al.* 1981). Tissue shrinkage was estimated from the histological material of several brains that had landmark lesions placed in the lateral geniculate nucleus during recording and that were processed for histology as described above. The average shrinkage was roughly 20 % linearly, and although variability was seen in these estimates, we corrected our final measures of HRP-labelled cells for this average shrinkage (see also Discussion).

Electron microscopy. We made some measurements of dendritic diameters from electron microscopic material. This was performed to improve the resolution (to roughly 0·05 μm) for the thinner, more distally located dendritic segments. The actual measurements were made from serial reconstructions of dendritic arbors that were photographed and then printed at a magnification of 8500 ×. These reconstructions are part of another study (Hamos *et al.* 1986), and details of the tissue preparation for electron microscopy can be found elsewhere (Wilson *et al.* 1984).

Statistics

Unless indicated otherwise, statistical analyses were made using the Mann–Whitney *U* test (Krauth, 1983).

RESULTS

We obtained data from seventy-four geniculate X and Y cells during the course of these experiments. Our morphometric analysis was based on measurements from fifty-four physiologically identified geniculate neurones that were subsequently labelled with HRP. Plate 1 shows representative examples of HRP-labelled geniculate cells. Of these labelled neurones, thirteen were used for measurements of dendritic morphology, and the remaining forty-one were used for the determination of A_n. The biophysical measurements were from twenty-eight cells whose intracellular records met the criteria outlined in Methods. Eight of the fifty-four HRP-labelled cells used for morphological analysis of A_n were among the twenty-eight studied biophysically.

Assumptions of the equivalent cylinder model

The equivalent cylinder model that we used in the analysis of the passive electrical properties of geniculate neurones has several underlying assumptions (Rall, 1959*b*, 1970, 1977). In addition to previously established assumptions basic to axonal electrotonus (Hodgkin & Rushton, 1946; Davis & Lorente de No, 1947) these assumptions include: (1) that the internal surface of the somatic membrane is isopotential, allowing the soma to be represented as a lumped impedance; (2) that the external resistance is uniform and negligible over the external surface of the entire neurone; (3) that all electrical properties, including specific membrane and internal resistance, are constant throughout the cell; (4) that all terminal endings are of the

same form (i.e. sealed, infinite resistance); (5) that the pattern of dendritic branching conforms to the '$\frac{3}{2}$ power rule'; (6) that all terminal branches end at the same total electrotonic distance from the soma; and (7) that current flows passively within the dendritic arbor. Detailed expositions of the underlying assumptions of the model have been presented elsewhere (Rall, 1959*b*, 1970, 1977; Jack *et al.* 1975; Iansek & Redman, 1973). Although we could not test experimentally most of these underlying assumptions, we have at least examined partially the validity of the last three as applied to geniculate neurones. The morphological and electrical constraints of dendritic branching are considered in the following section, and the requirement of passive current flow is discussed below under 'Biophysical measurements'.

Morphometry

Patterns of dendritic branching. The reduction of a dendritic tree to an equivalent cylinder requires that, at each dendritic branch point, the sum of diameters of the daughter dendrites (D_d) taken to the $\frac{3}{2}$ power equals the diameter of the mother dendrite (D_m) taken to the $\frac{3}{2}$ power (Rall, 1959*a*):

$$D_m^{\frac{3}{2}} = \Sigma D_d^{\frac{3}{2}}. \tag{9}$$

We tested this relationship at ninety-seven branch points (thirty-nine from Y cells and fifty-eight from X cells) from ten different HRP-labelled geniculate neurones. We purposely made measurements from a population of cells that displayed considerable morphological variability (e.g. Friedlander *et al.* 1981) to avoid any pronounced bias in favour of any one class of cell. One complication of the measurements was that the dendrites of geniculate neurones, particularly those of X cells, exhibited numerous swellings and constrictions along a single branch. Therefore, for each dendritic segment showing such irregularities, an average diameter was calculated from measurements made each 3–5 μm. Of the ninety-seven branch points, seventy-six were mostly proximal and thus of large calibre, and we measured their diameters with the light microscope. To ensure accurate measures at distal locations, where dendritic diameters approach the resolution of the light microscope, twenty-one additional branch points were studied by using material reconstructed from the electron microscope.

Fig. 1 illustrates the data from all ninety-seven branch points, including proximal, intermediate, and distal locations. It is clear from these data that both X and Y cell dendritic arbors follow the '$\frac{3}{2}$ power rule' remarkably well. This pattern of dendritic branching consequently fits the geometrical requirement for the reduction of these dendritic arbors to equivalent cylinders. Although the scatter in the data may indicate intrinsic differences among individual branch points, it may simply reflect the error in our measurements, particularly for those branches that displayed considerable variation in diameter.

Electrotonic lengths of terminal branches. An additional constraint must be met before a dendritic tree can be collapsed into an equivalent cylinder. Namely, all terminal branches that derive from a single primary dendrite end at the same electrotonic distance from the soma. We tested this constraint, as far as our methods allow, on arbors emanating from six primary dendrites, one from each of three X and three Y cells. Given the assumptions of constant specific membrane and internal

resistances (see above), the electrotonic length of an individual dendritic segment is proportional to $l/\sqrt{d}$, where l is the actual length of the segment and d is its diameter. The electrotonic length along a dendritic path is simply the sum of the electrotonic lengths of the individual segments traversed. We used this algorithm to calculate the electrotonic distance to the soma from each terminal ending of a dendritic arbor.

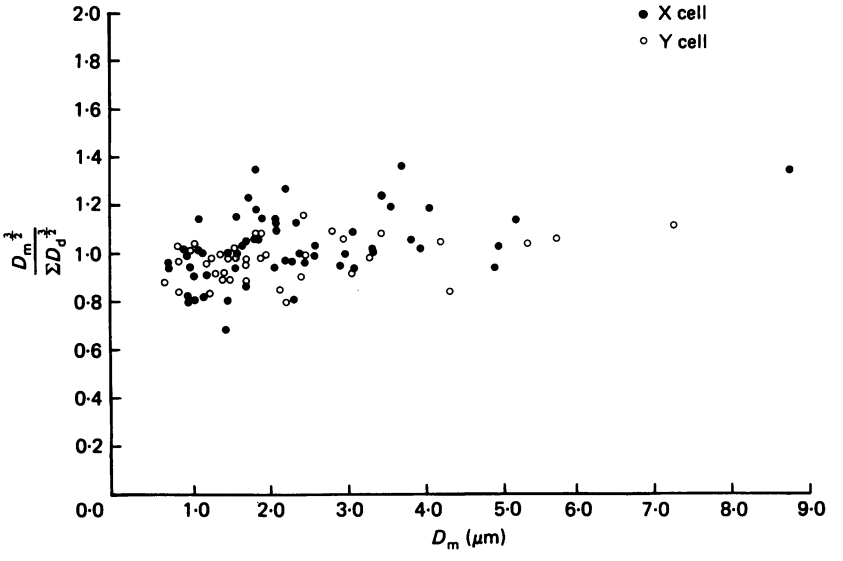

Fig. 1. Analysis of the $\frac{3}{2}$ power rule at ninety-seven dendritic branch points of ten different HRP-labelled geniculate neurones. The ordinate expresses the $\frac{3}{2}$ power relationship, and the abscissa reflects the diameter of the mother dendrite (D_m). Measurements of diameters of proximal dendrites were mostly made with the light microscope, whereas analysis of distal branch points were made from material reconstructed with the electron microscope (see text). Dendritic branch points of both X and Y cells satisfy the $\frac{3}{2}$ power rule remarkably well, exhibiting an average value of $0{\cdot}99 \pm 0{\cdot}13$ for this relationship.

The arbors from these primary dendrites provided between six and sixteen such terminal endings, with a mean of 10·8. The values of electrotonic distance for each arbor were normally distributed. To test whether the electrotonic distances of the terminal branches within a single arbor were equivalent, we compared the variance of these values with that expected from measurement error alone (Mendenhall & Scheaffer, 1973). We assumed a measurement error of 0·5 μm for diameter and 4 μm for length; diameter measurements reflect only the resolution limit of the light microscope, whereas length measurements also reflect errors in extracting three-dimensional information from our histological sections. Using χ^2 statistics, we found that the variance in values of terminal electrotonic distances for each arbor was equal to or less than the measurement error ($P < 0{\cdot}08$–$0{\cdot}15$ for all arbors). Consequently, within the limitations of our histological measures, these data suggest that dendritic terminals emanating from a single primary dendrite have equally long electrotonic paths to the soma.

Although geniculate cells often contain primary dendrites that produce arbors of varying size, data presented in a succeeding section of Results indicate that larger

arbors are associated with thicker dendrites and thus larger space constants. Indeed, our impression is that all dendritic endings for a single cell related to different primary dendrites exhibit similar electrotonic distances from the soma. We obtained limited data to support this impression. For two additional neurones (one X and one Y cell), measurements of terminal electrotonic distances were made from two dendritic arbors each. For the X cell, these primary dendrites produced eight and nine terminal endings, and the mean electrotonic distance between the endings of one primary dendrite and the soma were not significantly different from those of the other ($P > 0{\cdot}1$). Likewise, the primary dendrites for the Y cell provided fifteen and thirteen endings, with no significant difference between the electrotonic distances of these endings from the soma ($P > 0{\cdot}1$).

These measurements of electrotonic distance between terminal endings and soma, while limited in scope and subject to error, none the less suggest that dendritic arbors of a geniculate cell can be reduced to equivalent cylinders of equal L.

Membrane surface area. To determine the R_m of geniculate neurones, it was necessary to measure the somatic–dendritic membrane surface area (A_n) of these cells in addition to their electrical parameters (see eqn. (7)). This required the intracellular labelling of cells with HRP following the analysis of cable properties. Unfortunately, a direct measurement of A_n is a tedious and time-consuming task, requiring estimates of diameter and length of many segments of the dendritic tree. However, a much simpler solution to this problem has recently been suggested. In a study of spinal motoneurones, Ulfhake & Kellerth (1981) and Ulfhake & Cullheim (1981) found a strong linear relationship between the diameter of the primary dendrite and the total membrane surface area of all dendritic segments deriving from that dendrite. Burke, Dum, Fleshman, Glenn, Lev-Tov, O'Donovan & Pinter (1982) subsequently generated an algorithm from these data with which they could calculate the surface area of any motoneurone's dendritic arbor simply by measuring the diameters of its primary dendrites.

We adopted a similar strategy in our measurements of A_n for geniculate neurones. Fig. 2 shows drawings of single dendritic branches reconstructed from an HRP-labelled X and Y cell, and Pl. 1 *A* and *B* shows photomicrographs of these branches. The dendritic branches were divided into individual segments that were represented as smooth cylinders with uniform diameter (Fig. 2*B* and *D*). The diameter and length of each segment were determined with careful attention paid to the movement of processes in and out of the plane of section in order to incorporate all three dimensions into our measurements. From these measurements, we calculated the membrane surface area of each dendritic segment.

In this fashion, we laboriously determined the membrane surface area of all of the dendritic arbor related to thirteen primary dendrites. These were selected from a heterogeneous population of thirteen different cells (seven X and six Y cells) to minimize any bias in our measurements for any one morphological class. Fig. 3 shows the relationship between the diameter of the primary dendrite and the total membrane surface area of all dendritic arbor related to it. Since these values are highly correlated ($r = +0{\cdot}99$; $P < 0{\cdot}001$), we could fit a line to the points by the method of least squares. The line's equation, $y = 1{\cdot}68x - 0{\cdot}99$, provided an algorithm for the determination of the membrane surface area (y) of a dendritic arbor from the

diameter of its primary branch (x). Both X and Y cells follow this linear relationship with the same algorithm, indicating a common aspect to the architecture of their dendritic arbors. Interestingly, this algorithm differs from that reported by Burke *et al.* (1982) for motoneurones. We could now calculate the dendritic surface areas

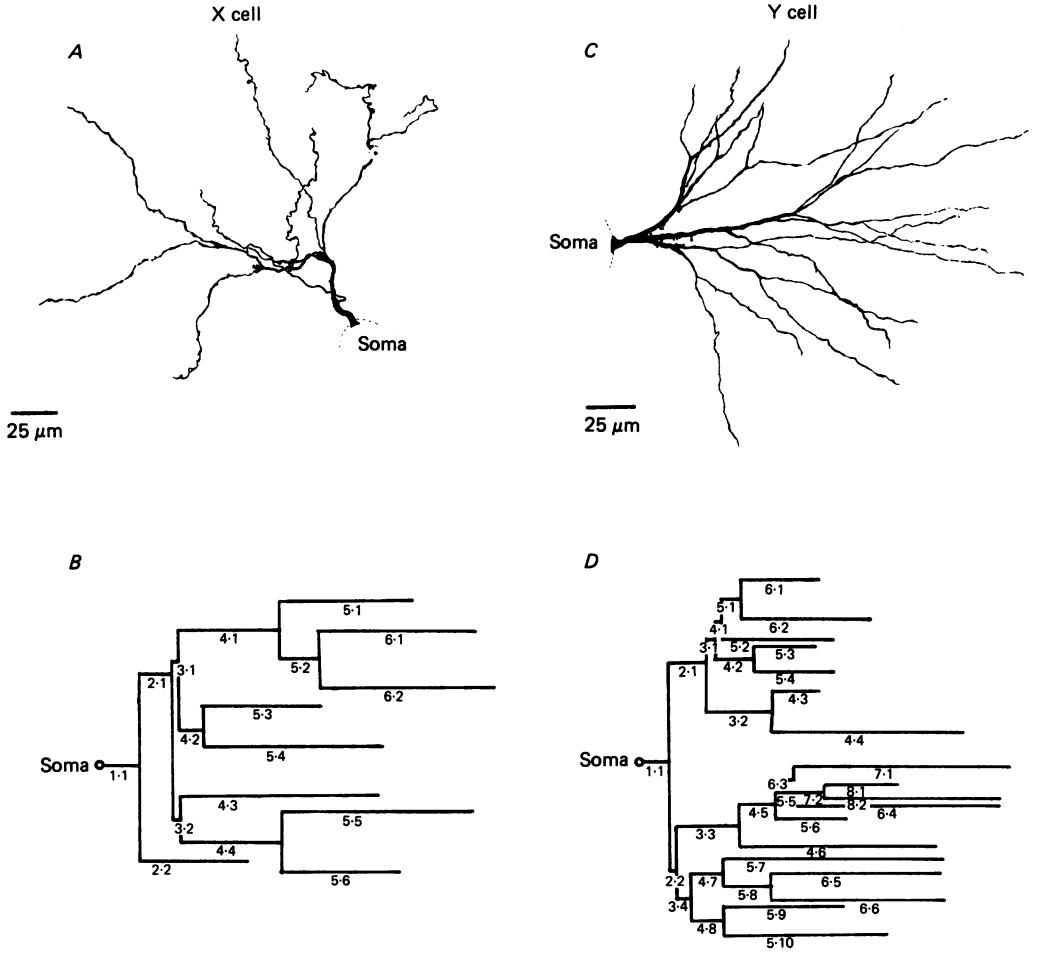

Fig. 2. Reconstructions of all dendritic processes emanating from a single primary dendrite for a geniculate X and Y cell labelled with HRP; coronal views. *A*, reconstruction for an X cell. *B*, Sholl plot of the same arbor shown in *A*. The arbor was divided into individual segments and measurements of both length and diameter were made for each to determine the total membrane surface area of the arbor. The length of each segment in the Sholl plot reflects the actual length of the dendritic segment it represents. *C*, reconstruction for a Y cell. *D*, Sholl plot of the arbor illustrated in *C*; conventions as in *B*.

of geniculate neurones by simply measuring the diameters of all primary dendrites and sequentially applying the derived algorithm. Furthermore, this new method permitted the use of less-well-labelled cells in which only the proximal dendrites were darkly stained.

To determine A_n, the somatic membrane surface area must also be calculated. We

estimated the somatic membrane surface area by assuming the soma to be spherical with a diameter equal to the average of its maximum diameters measured in the x, y and z planes. More elaborate calculations, including a correction for the surface area occupied by the bases of primary dendrites, were not made since the somatic surface area accounted for $< 10\%$ of the total A_n of our sample of cells.

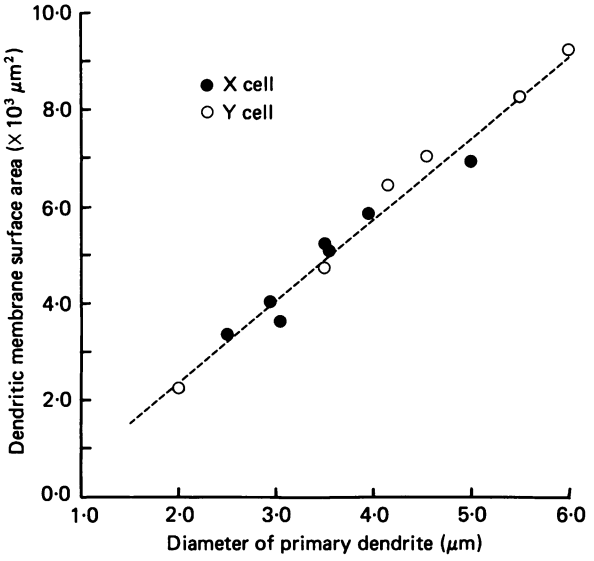

Fig. 3. Graph illustrating the relationship between the membrane surface area of dendritic arbors emanating from single primary dendrites, as illustrated in Fig. 2, and the diameter of the corresponding primary dendrites. Measurements were made from thirteen different HRP-labelled geniculate cells. The coefficient of correlation for these data is 0·99, indicating a strong linear relationship. A best fit line was generated for these data using the method of least squares (dashed line). The equation $y = 1{\cdot}68x - 0{\cdot}99$, allowed us to calculate the membrane surface area (y) of all dendritic processes related to a primary dendrite from the diameter of the primary dendrite (x).

By these methods, we estimated A_n for forty-one other geniculate neurones, including twenty-two HRP-labelled X and nineteen Y cells (Fig. 4*A*). The A_n for X cells ranged from 19900 to 46200 μm^2 (with a mean $\pm$ S.D. of 32700 $\pm$ 8300 μm^2), whereas the values for Y cells were 33300 to 55200 μm^2 (44000 $\pm$ 6500 μm^2). Although there is overlap in A_n values between the two classes, on average Y cells are clearly larger than X cells ($P < 0{\cdot}001$).

Fig. 5 illustrates another feature of these membrane surface area measurements. For each neurone, the surface area of the soma is highly correlated with its total A_n. This is as true of the entire cell population as it is for X and Y cells individually ($r = +0{\cdot}87$ to 0·92 and $P < 0{\cdot}001$ for all correlations). This confirms an earlier conclusion, based on different morphometric measurements, that larger somata of geniculate neurones are related to more extensive dendritic arbors (Friedlander *et al.* 1981; Stanford *et al.* 1983).

Scaling of dendritic arbors. Fig. 6 illustrates yet another feature of dendritic branching for these geniculate X and Y cells. A strong relationship exists between

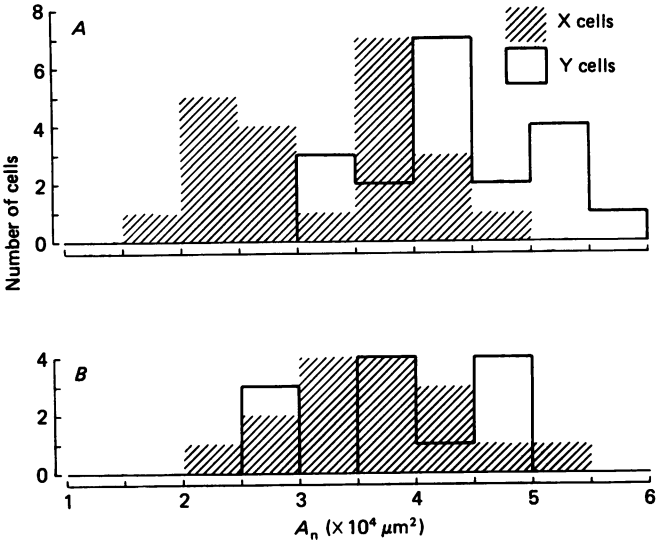

Fig. 4. Measurements of the total somatic–dendritic membrane surface areas of geniculate X and Y cells. *A*, A_n for forty-one HRP-labelled geniculate X and Y cells based on morphological measurements. Although there is clear overlap in the A_n values for the two classes, on average Y cells are larger than X cells. *B*, distribution of A_n values for twenty-eight geniculate X and Y cells derived entirely from their passive electrical properties using eqn. (11) (see text).

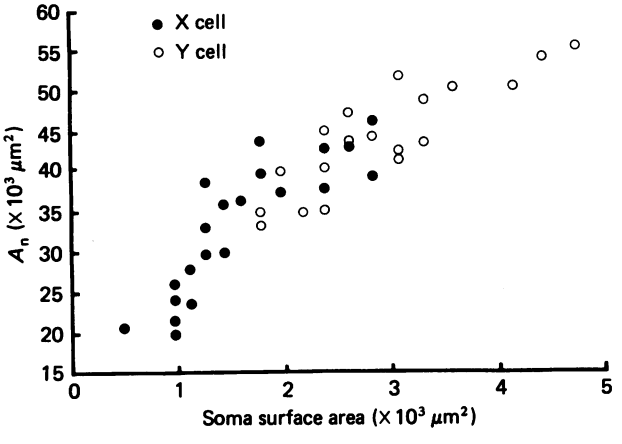

Fig. 5. Relationship between the total somatic–dendritic membrane surface areas (A_n) of geniculate cells and the surface areas of their somata.

the diameter of the primary dendrite and both the total number of branch points in the resultant arbor (Fig. 6*A*) as well as the total number of dendritic segments in that arbor (Fig. 6*B*). The similarity in the two relationships of Fig. 6*A* and *B* is not surprising inasmuch as each parent dendrite always gave rise to two daughter dendrites at branch points. These relationships of Fig. 6*A* and *B* are statistically significant ($r = +0{\cdot}91$, $P < 0{\cdot}001$ for all of the neurones; $r = +0{\cdot}74$, $P < 0{\cdot}05$ for the

X cells and $r = +0{\cdot}95$, $P < 0{\cdot}001$ for the Y cells). Interestingly, these correlations are stronger for Y cells than for X cells ($P > 0{\cdot}02$ on a comparison of correlation coefficients), which implies that the arbors of Y cells are simply scaled versions of one another, with larger primary dendrites giving rise to predictably more daughter branches and higher-order dendritic segments. In contrast, X cells have more heterogeneity in the geometry of their dendritic arbors than do Y cells. These are themes to which we shall return repeatedly below.

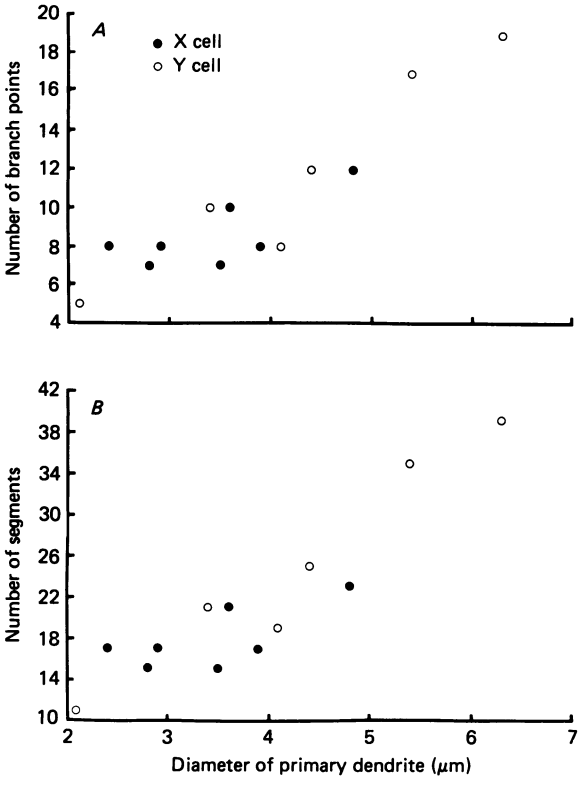

Fig. 6. Relationship between the diameter of the primary dendrite and the number of segments and branch points in the resultant arbor. The data were taken from the thirteen HRP-labelled dendrites illustrated in Fig. 3. *A*, scatter plot illustrating the strong correlation for both X and Y cells between the diameter of the primary dendrite and the number of branch points in the resultant arbor. *B*, scatter plot illustrating a similar strong correlation between the diameter of the primary dendrite and the number of segments in the resultant arbor.

Biophysical measurements

We studied the passive membrane properties of twenty-eight geniculate neurones (sixteen X and twelve Y cells) that met our criteria for adequate intracellular recording (see Methods). Nineteen of these cells were unequivocally identified as relay neurones based upon the ability to activate them antidromically from visual cortex or clear visualization of an axon entering the optic radiations following HRP

labelling. The remainder had similar response properties, and we assume that most or all were relay cells, although for these we employed neither antidromic activation nor HRP labelling. Fig. 7 illustrates an intracellular recording from a geniculate X cell, exemplary of the quality of recordings obtained during this study. This cell exhibited a steady resting membrane potential of −67 mV with spike amplitudes of approximately 60 mV. These recordings were obtained during the presentation of a counterphased sinusoidal grating. Fig. 7*A* shows the lack of a modulated response to a grating placed at the null position, and Fig. 7*B* shows the modulated and linear response of this cell when the same grating was displaced from the null position by 90 deg.

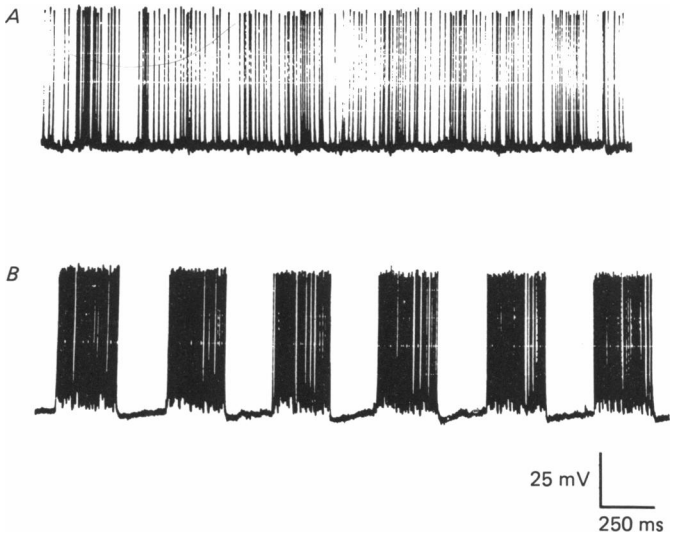

Fig. 7. Intracellular recording from a geniculate X cell. These records were obtained during visual stimulation with a grating sinusoidally modulated in space and time. The grating was generated on a cathode ray tube; it had an average luminance of 40 cd/m² and a maximum contrast of 0·6. *A*, lack of a modulated response of this neurone to a grating placed in the null position of the receptive field of this cell. Note the high spontaneous activity of this cell. *B*, linear response of this neurone to the same grating when spatially displaced by a phase angle of 90 deg from the null position.

Current–voltage (I–V) relationships. As noted earlier, a major assumption of the equivalent cylinder model is that current flow within the dendritic tree is totally passive. As a partial test of this assumption, we studied the *I–V* relationships for ten geniculate neurones (five X and five Y cells), paying particular attention to any non-linearities indicative of rectification induced by voltage-dependent conductances. Fig. 8 illustrates the *I–V* curves for an X and a Y cell showing no obvious non-linearities for a voltage range of ±20 mV from the resting potential. The *I–V* curves for the other X and Y cells were quite similar to those illustrated in Fig. 8. The decrease in R_n (slope of *I–V* curve) seen during the greatest depolarization probably reflects activation of voltage-sensitive sodium channels, since action potentials were usually initiated at or near this level. The R_n values obtained from

the slope of the I–V relationships of Fig. 8 were 18 MΩ for the X cell and 13 MΩ for the Y cell. This is consistent with R_n measurements from other geniculate neurones (see below). Of course, the data do not rule out absolutely the existence of additional active conductances in these cells, because non-linear mechanisms of opposite polarity can conceivably cancel one another and remain undetected in measurements such as those depicted in Fig. 8. Voltage- and time-dependent conductances have

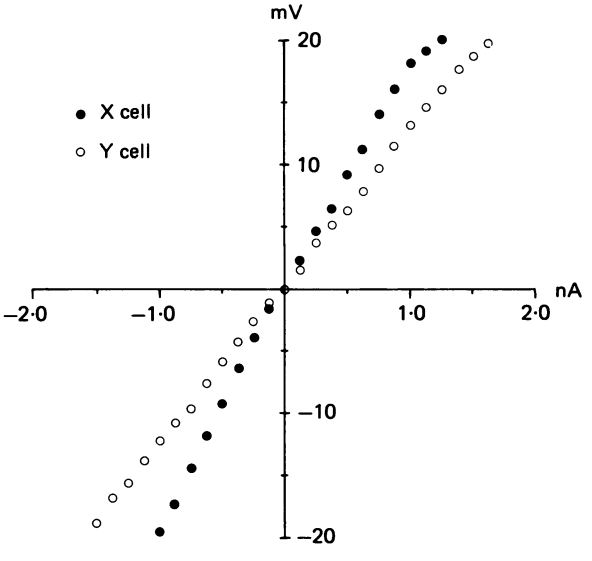

Fig. 8. Current–voltage (I–V) relationships for a geniculate X and Y cell. These data were obtained using 250 ms duration current pulses delivered through the intracellular recording electrode. The resting membrane potentials were −64 mV for the Y cell and −62 mV for the X cell. There are no obvious non-linearities in the I–V curves for either the X or the Y cell, thereby implying that no voltage-dependent conductances were activated in a range of ±20 mV from the resting membrane potential of these cells.

been described for mammalian thalamic cells (Jahnsen & Llinás, 1984*a*, *b*; Deschenes, Paradis, Roy & Steriade, 1984; Roy, Clercq, Steriade & Deschenes, 1984), but the 50 ms duration of most of our current injections is probably too brief to activate many of these. For instance, the calcium conductance underlying a low-threshold spike requires a 100–200 ms period of hyperpolarization before it can be de-inactivated (Jahnsen & Llinás, 1984*a*, *b*).

The relatively large voltage range about the resting membrane potential for which geniculate neurones appeared to behave passively meant that we could easily remain within these limits during analysis of voltage transients. Furthermore, as described in Methods, such analysis was carried out on four cells with both 50 ms (long) and 0·5 ms (short) current pulses. Durand *et al.* (1983) have recently suggested that short current pulses reduce the possibility of activating time-dependent conductances (e.g. Ito & Oshima, 1965). Therefore, a comparison between these two protocols provides a second test for non-linear behaviour of geniculate cells. In each case (two X and two Y cells), we found no significant difference between the time constants

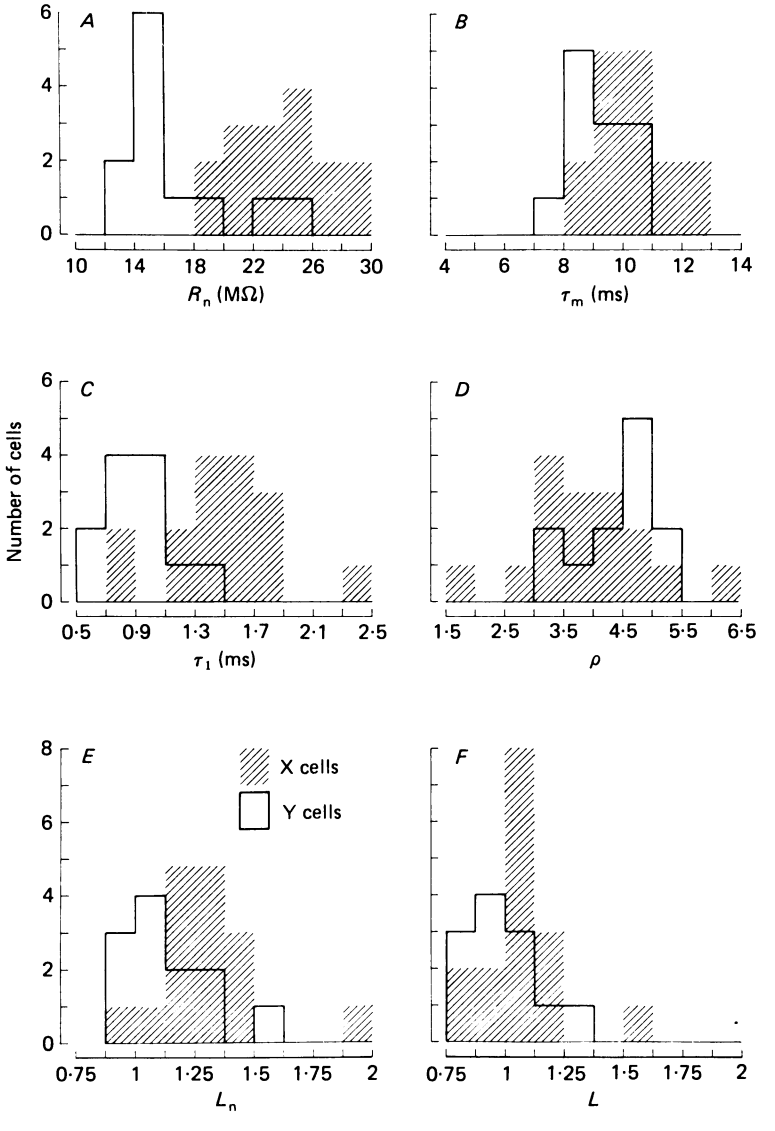

Fig. 9. Distributions of the passive membrane properties of sixteen X cells and twelve Y cells in the lateral geniculate nucleus. *A*, frequency histograms of values for input resistance (R_n). *B*, frequency histograms of values for membrane time constant (τ_m). *C*, frequency histograms of values for first equalizing time constant (τ_1). *D*, frequency histograms of values for dendritic-to-somatic conductance ratio (ρ). *E*, frequency histograms of values for the whole neurone electrotonic length (L_n). *F*, frequency histograms of values for the electrotonic length (L) of the equivalent cylinder representing only the dendritic arbor.

obtained using either long or short pulses, thus providing further evidence for the passive and linear behaviour of these geniculate cells during our recording conditions.

Input resistance (R_n). R_n of each geniculate neurone was measured using constant current pulses of $\pm 0{\cdot}25$ nA. Fig. 9*A* shows the distribution of R_n values. These values were greater for X cells (with a mean $\pm$ S.D. of $22{\cdot}6 \pm 3{\cdot}2$ MΩ) than for Y cells ($16{\cdot}0 \pm 3{\cdot}6$ MΩ), with distributions that are significantly different ($P < 0{\cdot}001$). This result is not surprising, given the smaller size of X cells, and does not, by itself, suggest any differences between X and Y cells with regard to their intrinsic membrane properties.

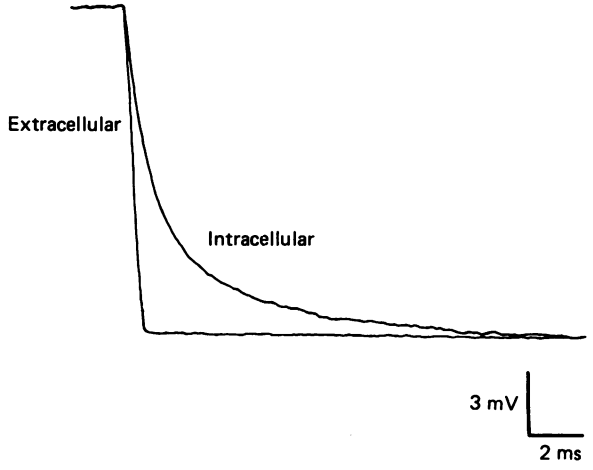

Fig. 10. Transient voltage responses to the onset of a 50 ms duration square-wave current pulse applied through the recording electrode. The faster response was obtained while the recording electrode was just extracellular to a geniculate X cell. The slower response was obtained while the electrode was intracellular to the geniculate X cell. The resting membrane potential was −59 mV. The amplitude of the current pulses was adjusted to produce voltage responses of equal amplitude. The response time of the electrode in extracellular space is clearly faster than it is in the neurone.

Membrane time constant (τ_m). τ_m of each geniculate neurone was measured from the voltage transient response to a constant current pulse. Fig. 10 illustrates two voltage responses to the same 50 ms square-wave current pulse applied through the amplifier bridge. The faster response was obtained while the electrode was just extracellular to a geniculate X cell, and the slower one was recorded while the electrode was inside the same X cell. The response time (i.e. the time needed for the voltage response to reach a steady, d.c. level) is considerably faster in the extracellular space than it is inside the cell. In fact, the time constants of our electrodes were typically at least two orders of magnitude shorter than the τ_m values of geniculate neurones and one order of magnitude shorter than the τ_1 values. Hence, we did not adjust our measures of neuronal time constants to account for the insignificant contribution of the electrodes.

The response of an X cell to a 50 ms current step of −0·5 nA can be seen in Fig. 11*A*. This cell exhibited a stable resting potential of $\simeq$ −59 mV, and its action

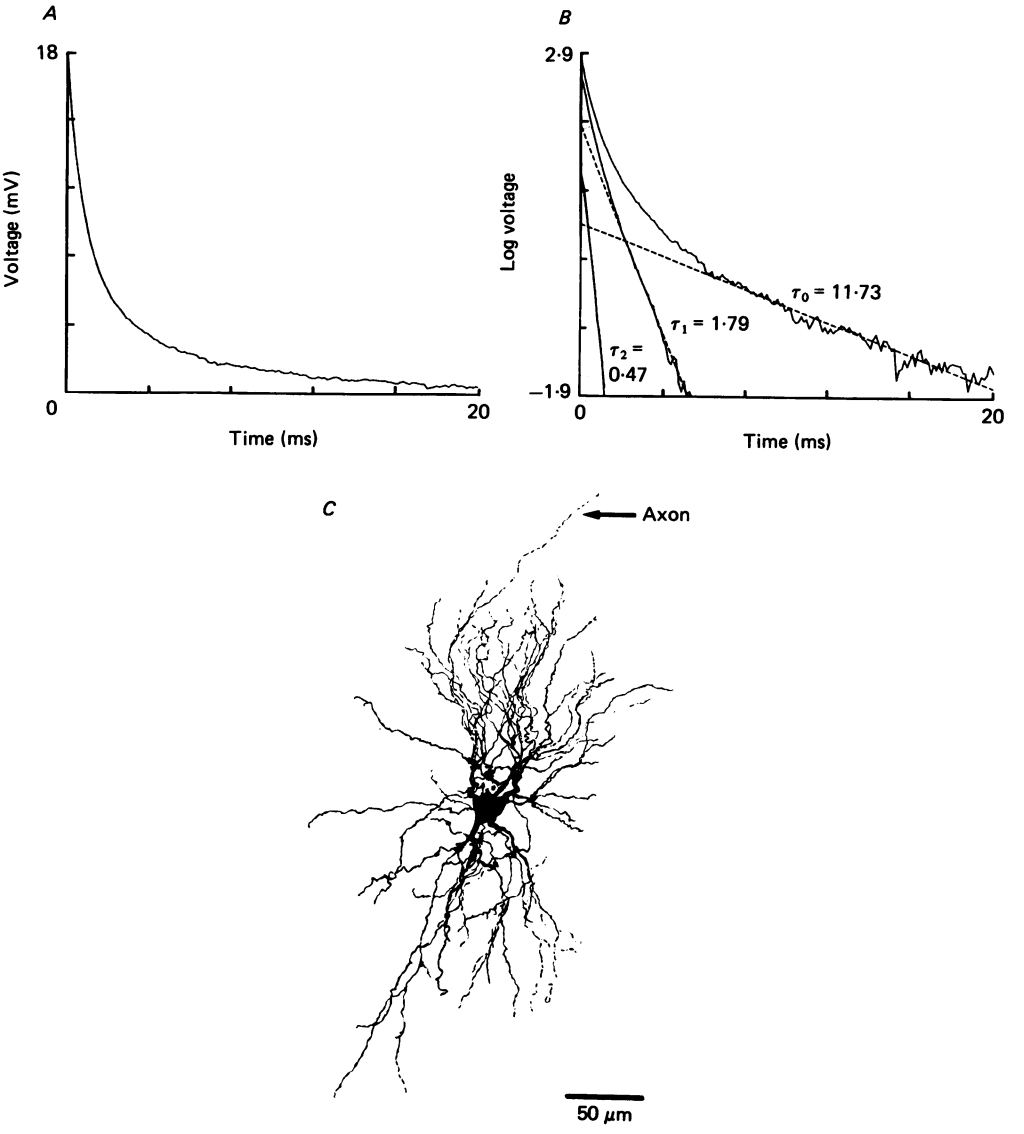

Fig. 11. Determination of the membrane and equalizing time constants of a geniculate X cell using the method of exponential peeling. *A*, computer average of 100 intracellularly recorded voltage responses to a 50 ms duration current pulse of −0·25 nA. The actual plot represents the voltage response as a function of time following the onset of the current pulse. *B*, same data as in *A* except the ordinate has been converted to the natural logarithm of the voltage. The final linear portion of the curve was fitted by a least-squares algorithm by computer, and this line was extrapolated to time zero. The negative reciprocal of the slope of this line equals the membrane time constant ($\tau_0 = \tau_m = 11{\cdot}73$ ms). Subtraction of this line from the short latency exponential portion of the curve yields a second curve, for which the process of fitting a line to its linear portion is repeated. The first equalizing time constant ($\tau_1 = 1{\cdot}79$ ms) is derived from the negative reciprocal of the slope of this second line. Further peeling in this manner leads to derivation of the second equalizing time constant ($\tau_2 = 0{\cdot}47$ ms). In practice, we could never clearly resolve time constants beyond τ_2. However, only τ_m and τ_1 were important for our computations (see text). *C*, drawing of the HRP-labelled X cell from which the electrical data described in *A* and *B* were obtained; coronal view.

potentials were 40 mV in amplitude. A plot of the natural logarithm of the voltage against time (Fig. 11*B*) reveals both exponential and linear portions of this function, thereby indicating a multi-exponential decay. τ_m (which equals τ_0) and τ_1 and τ_2 were determined by sequentially 'peeling' the linear component from the exponential portion of the curve. This X cell displayed a τ_m value of 11·73 ms, τ_1 of 1·79 and τ_2 of 0·47 ms. We subsequently ionophoresed HRP into this neurone, and a reconstruction of the labelled cell is illustrated in Fig. 11*C*. The cell body was located in lamina A. Its morphology, including numerous dendritic appendages and a dendritic arbor oriented mostly at right angles to the borders of lamina A, is typical of that of X cells (Friedlander *et al.* 1981). The A_n for this neurone was 43700 μm^2, making it one of the largest X cells in our sample (see Figs. 4 and 5).

A similar analysis for a Y cell is illustrated in Fig. 12. This cell, whose soma was located in lamina C, had a resting potential of −58 mV and exhibited action potentials with amplitudes of 32 mV. Its τ_m was 9·67 ms, which is slightly shorter than that measured for the X cell, τ_1 was 0·95 ms and τ_2 was 0·20 ms. The cell was also labelled with HRP and displayed an A_n of 50400 μm^2 (Fig. 12*C*). This cell exhibited typical Y cell morphology, including fairly straight, smooth dendrites and a roughly spherical geometry to its dendritic arbor (Friedlander *et al.* 1981).

As shown in Fig. 9*B*, the total population of X cells exhibited longer and somewhat more variable τ_m values than did Y cells (with means ± S.D. for X cells, 10·28 ± 1·30, and for Y cells, 8·15 ± 0·81 ms). This difference between X and Y cells is statistically significant ($P < 0.001$ for a test of the difference of means; $P < 0.05$ on an F test for the difference of variance) and suggests differences between the intrinsic membrane properties of X and Y cells. Indeed, data to be described below suggest that the difference in τ_m between the two neuronal classes reflects a higher and more variable R_m for X cells than for Y cells.

Equalizing time constants (τ_i). τ_i values reflect the time needed to redistribute current within the neurone so that the membrane can return to a state of isopotentiality. These time constants depend somewhat on the geometry of the cell's dendritic arbor, and they thus provide some measure of this dendritic geometry. Our methods routinely can resolve only the first two equalizing time constants, and to be conservative, we have analysed in detail only the first of these (τ_1) for X and Y cells (Fig. 9*C*). It is interesting that these values for X cells (with a mean ± S.D. of 1·48 ± 0·40 ms) are longer than for Y cells (0·90 ± 0·22 ms). This difference is statistically significant ($P < 0.001$). There is also more variance in the values for X cells than for Y cells ($P < 0.01$ on an F test). We found no evidence that the τ_1 values were an epiphenomena of the τ_m values because, within each neuronal class, these values were uncorrelated ($r = +0.31$, $P > 0.1$ for X cells, and $r = -0.06$, $P > 0.1$ for Y cells). Thus the τ_1 values may be regarded as independent evidence of intrinsic differences between X and Y cells, perhaps related to the above-mentioned morphological differences in dendritic branching patterns for these cell types.

Dendritic-to-somatic conductance ratio (ρ). ρ was calculated for twenty-eight cells using the method formulated by Brown *et al.* (1981*a*). The X and Y cells displayed similar values of ρ that were not statistically different (Fig. 9*D*; mean ± S.D. for X cells, 3·89 ± 1·00 and for Y cells, 4·34 ± 0·70; $P > 0.1$). The similarity in ρ between

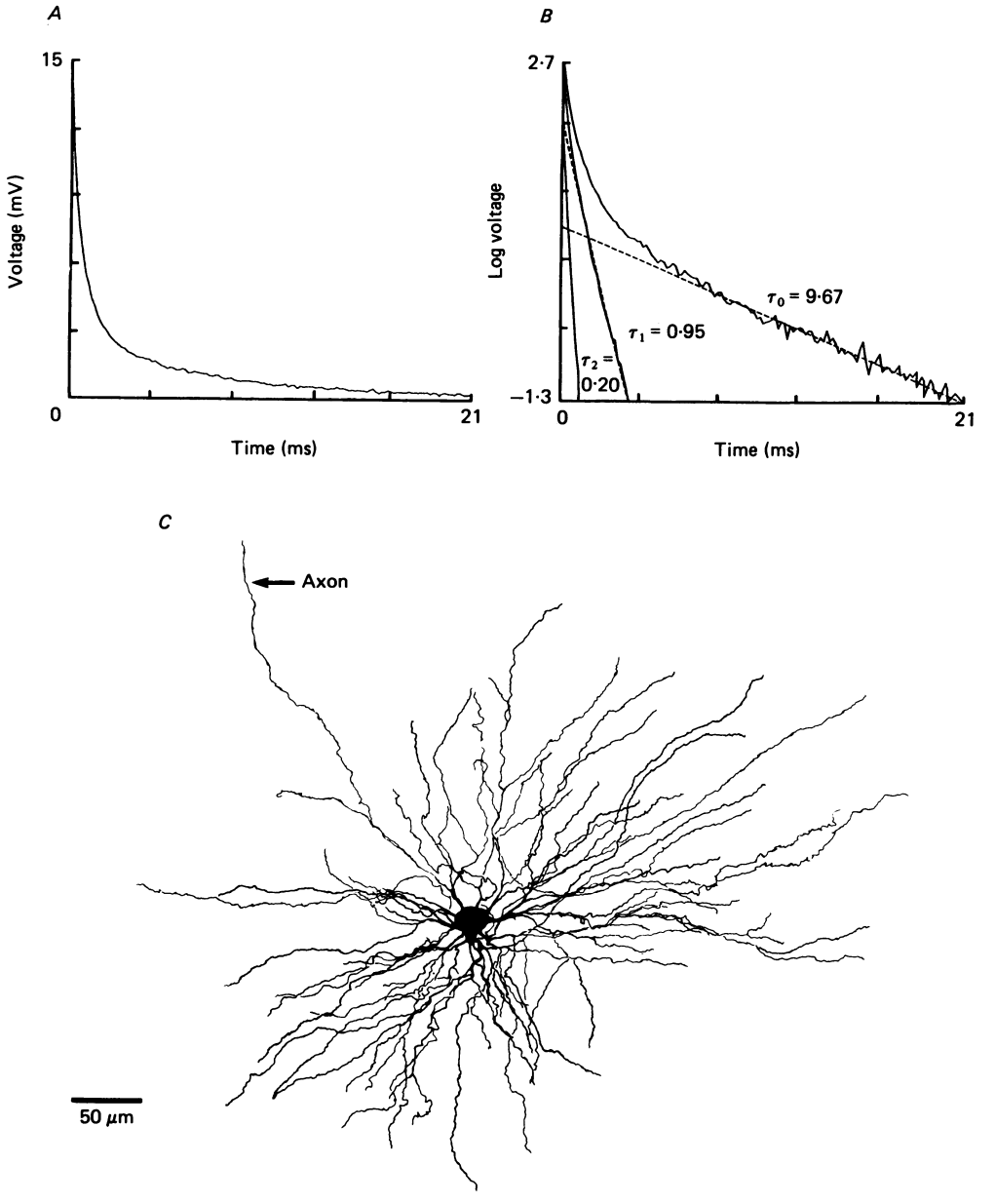

Fig. 12. Determination of the membrane and equalizing time constants for a geniculate Y cell using the method of exponential peeling; procedure and conventions as in Fig. 11. *A*, computer average of 150 intracellularly recorded voltage responses to a −0·25 nA current pulse of 50 ms duration. *B*, same data as in *A* except the ordinate has been converted to the natural logarithm of the voltage. Exponential peeling of this curve yields the membrane time constant ($\tau_0 = \tau_m$ = 9·67 ms) plus the first and second equalizing time constants (τ_1 = 0·95 and τ_2 = 0·20 ms). *C*, drawing of the HRP-labelled Y cell from which the data in *A* and *B* were obtained; coronal view.

classes as well as the small variance in these values was surprising in light of the tremendous variability in soma size and dendritic geometry of geniculate neurones.

Rall (1959*b*) has shown that ρ can also be roughly estimated from the relationship:

$$\rho = 0{\cdot}2\,(R_m)^{\frac{1}{2}}(\Sigma d^{\frac{3}{2}})/A_s, \tag{10}$$

where d is the diameter of each primary dendrite and A_s is the surface area of the soma. This equation implies that ρ is proportional to R_m as well as the ratio of the size parameters for the primary dendrites ($\Sigma d^{\frac{3}{2}}$) and soma (A_s). As shall be demonstrated below, X cells are endowed with slightly higher values of R_m than are Y cells. Thus the fact that the cell classes exhibited similar values of ρ implies that the ratio $\Sigma d^{\frac{3}{2}}/A_s$ is smaller for X cells than for Y cells.

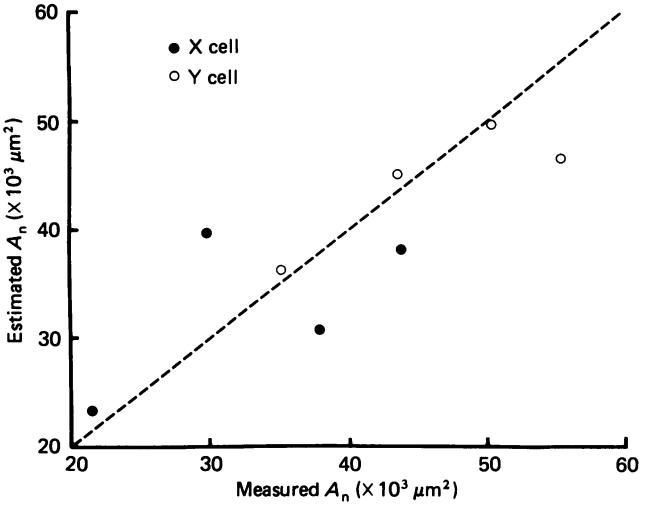

Fig. 13. Comparison of morphologically determined and biophysically derived total membrane surface areas (A_n) of geniculate X and Y cells. Each of the eight cells represented in this data was labelled with HRP and biophysically analysed. The abscissa represents the morphologically determined A_n, and the ordinate indicates the A_n values derived entirely from electrical properties (see text). The dashed line, which has a slope of 1, is shown for reference only.

Our morphological data support this contention. Data from our reconstructions of dendritic arbor related to thirteen primary dendrites (see Fig. 6) indicate that Y cells display, on average, thicker primary dendrites than X cells (4·3 μm for Y cells *versus* 3·4 μm for X cells). In addition, measurements from forty-one HRP-labelled geniculate neurones show that Y cells, on average, maintain more primary dendrites than do X cells (6·9 for Y cells *versus* 5·3 for X cells). With our estimates of A_s, we conclude that the size ratio $\Sigma d^{\frac{3}{2}}/A_s$ for Y cells is roughly 1·1 times that of X cells, which closely parallels the X to Y cell ratio of R_m of about 1·2. In essence, these data indicate that the greater R_m of X cells is roughly compensated by the larger $\Sigma d^{\frac{3}{2}}/A_s$ value of the Y cells, resulting in similar values of ρ for the two functional classes.

Electrotonic length (L). The electrotonic length of the entire neurone (L_n), which corresponds to that of the equivalent cylinder representing the dendritic arbor and

soma, was calculated from τ_m and τ_i (see eqn. (3)). Fig. 9*E* summarizes the L_n values. L_n was slightly but significantly greater for X cells than for Y cells (mean ± S.D. for X cells, 1·29 ± 0·21, and for Y cells, 1·10 ± 0·18; $P < 0·02$). Furthermore, the variance in L_n for X cells was greater than that for Y cells ($P < 0·001$ on an F test). A more exact value for L of the equivalent cylinder representing only the dendritic arbor was

TABLE 1. Electrical and morphometric parameters of geniculate neurones

Class	τ_m (ms)	τ_i (ms)	R_m (Ω cm²)	R_n (MΩ)	L_n	L	ρ	Estimated A_n ($\times 10^3$ μm²)	Measured A_n ($\times 10^3$ μm²)	C_m (μF/cm²)	V_m (mV)
X	9·91	1·32	5338	18	1·23	1·10	6·02	43·2	—	—	−55
X	9·31	2·49	5015	19	1·90	1·50	1·79	52·4	—	—	−52
X	9·71	1·63	5230	20	1·41	1·16	3·01	41·5	—	—	−62
X	10·14	1·78	5462	21	1·45	1·23	3·48	42·1	—	—	−69
X	12·89	1·74	6943	22	1·24	1·07	4·47	46·2	—	—	−54
X	8·60	1·31	5697	23	1·33	1·12	3·36	30·8	37·9	1·51	−62
X	9·44	1·42	5085	24	1·32	1·10	3·17	32·2	—	—	−61
X	11·73	1·69	6855	24	1·33	1·07	2·54	38·2	43·7	1·62	−59
X	9·49	0·78	5112	24	0·94	0·81	5·03	27·2	—	—	−54
X	10·62	1·82	5720	28	1·43	1·22	3·54	32·7	—	—	−67
X	8·90	0·82	4442	27	1·00	0·86	4·64	23·3	21·6	2·00	−65
X	10·38	1·21	5591	28	1·14	0·99	4·83	27·9	—	—	−56
X	9·79	1·13	5273	22	1·13	0·96	3·98	33·4	—	—	−55
X	10·00	1·37	4031	20	1·25	1·07	3·97	39·6	29·7	2·48	−55
X	11·32	1·57	6097	24	1·26	1·07	4·03	37·6	—	—	−67
X	12·35	1·60	6652	27	1·21	1·04	4·32	35·6	—	—	−54
Y	8·12	0·78	4374	16	1·02	0·88	4·72	36·2	35·1	1·92	−64
Y	7·02	1·30	3781	13	1·50	1·26	3·15	48·2	—	—	−60
Y	7·85	0·74	4228	14	1·01	0·88	4·85	39·8	—	—	−62
Y	8·00	1·09	4309	15	1·25	1·07	4·11	42·3	—	—	−63
Y	9·40	0·93	4880	15	1·04	0·90	4·73	45·1	43·5	1·93	−69
Y	9·67	0·96	5278	14	1·04	0·89	4·55	49·7	50·4	1·83	−58
Y	7·90	0·61	4255	18	0·91	0·80	5·23	29·8	—	—	−74
Y	7·83	1·22	4217	23	1·35	1·16	3·01	28·3	—	—	−60
Y	8·42	1·06	5394	14	1·19	1·02	4·21	46·4	55·2	1·56	−53
Y	9·65	0·75	5198	24	0·91	0·79	5·26	27·3	—	—	−56
Y	6·04	0·76	3253	12	1·19	1·01	3·72	38·8	—	—	−69
Y	7·87	0·65	4239	14	0·94	0·81	4·57	38·7	—	—	−51
Totals (mean ± S.D.)											
X	10·28 ± 1·30	1·48 ± 0·40	5534 ± 777	22·6 ± 3·2	1·29 ± 0·21	1·09 ± 0·15	3·89 ± 1·00	36·5 ± 7·3	33·2 ± 8·4	1·90 ± 0·38	−60·0 ± 5·5
Y	8·15 ± 0·81	0·90 ± 0·22	4451 ± 606	16·0 ± 3·6	1·10 ± 0·18	0·97 ± 0·16	4·34 ± 0·70	39·2 ± 7·3	46·1 ± 7·6	1·81 ± 0·15	−61·6 ± 6·5

determined by incorporating ρ into our calculations (see eqns. (5) and (6)). Fig. 9*F* shows that, as was the case for values of L_n, a small difference was observed in the measures of L (mean ± S.D. for X cells, 1·09 ± 0·15, and for Y cells, 0·97 ± 0·16; $P < 0·02$), with X cells exhibiting more variance than did Y cells on this measure ($P < 0·001$ on an F test).

Specific membrane resistance (R_m) and capacitance (C_m). Given the assumptions

required for the equivalent cylinder model that each neurone is endowed with a uniform R_m and C_m, R_m can be determined from knowledge of R_n, L and A_n (see eqn. (7)). Eight neurones were labelled with HRP after their biophysical properties were studied so that their A_n values could be calculated. On average, the X cells exhibited slightly higher and more variable R_m values than did the Y cells in this sample (mean $\pm$ S.D. for X-cells, $5256 \pm 1108\ \Omega\ cm^2$, and for Y cells, $4947 \pm 451\ \Omega\ cm^2$). However, possibly due to the small data base of four representative cells from each class, these differences between the X and Y cells are not statistically significant. C_m was then determined for these eight cells using eqn. (3). Values for C_m for both X and Y cells were quite similar, with the respective means for X and Y cells of 1·90 and 1·81 $\mu F/cm^2$; the mean $\pm$ S.D. of these values for all eight neurones was $1{\cdot}86 \pm 0{\cdot}29\ \mu F/cm^2$.

We assumed that geniculate neurones exhibit a common lipid basis for their membranes, which implies that C_m is constant across neurones. Using the derived average C_m value of $1{\cdot}86\ \mu F/cm^2$, we estimated A_n for each of the twenty-eight neurones from which cable properties were determined by substituting eqn. (8) into eqn. (7):

$$A_n = (\tau_m L_n)/[C_m R_n \tanh(L_n)]. \tag{11}$$

For each of the eight geniculate neurones that had their cable properties measured and that were labelled with HRP, A_n was derived from eqn. (11) and also measured more directly from histological material. Fig. 13 shows the strong correlation between these two measures ($r = +0{\cdot}83$; $P < 0{\cdot}01$). Fig. 4*B* shows the distribution of A_n values as derived from eqn. (11) for the twenty-eight X and Y cells from which cable properties were determined. These distributions are reasonably close to those determined from histological material and illustrated in Fig. 4*A* ($P < 0{\cdot}1$ on comparisons between histologically and biophysically derived A_n values for X and Y cells), although the size differences between X and Y cells of Fig. 4*B* are no longer statistically significant. However, Figs. 4 and 13 together support the validity of modelling neurones as cables to derive structure–function relationships. Finally, the average R_m value for all twenty-eight cells is $5534 \pm 777\ \Omega\ cm^2$ for X cells, and $4439 \pm 609\ \Omega\ cm^2$ for Y cells.

A summary of all electrical parameters of geniculate X and Y cells is given in Table 1.

Relationships among electrical parameters

In addition to determining the actual values for the various cable properties of geniculate neurones, we examined the interrelationships among these parameters. In particular, we were interested in which parameters were strongly predicted by the functional X or Y cell class, and which were more closely related to other neuronal properties.

Relationships with input resistance (R_n). The measurement of R_n can be influenced by several extrinsic factors. First, injury associated with electrode impalement can produce current shunts that effectively reduce the observed R_n values. Secondly, these shunts can lead to reduced resting membrane potentials that may, in turn, activate voltage-dependent conductances, resulting in further reductions in R_n. In

view of this, we examined what influence the resting membrane potential, which covered a range of 23 mV, had on R_n measurements. Any relationship between R_n and resting membrane potential could reflect shunting due to impalement injury, since both parameters would be conjointly reduced. Fig. 14 shows that no such relationship exists for either X and Y cells (for all cells, $r = -0{\cdot}08$; for X cells, $r = +0{\cdot}28$; for Y cells, $r = -0{\cdot}07$; $P > 0{\cdot}1$ for all correlations). Although we found no evidence of impalement injury, we none the less assume that cells were injured to some degree, because recent work has uncovered cell damage during even the highest quality recordings Durand *et al.* 1983; Gustafsson & Pinter, 1984). However, we feel that any cell damage during the present study was relatively small and not biased in favour of X or Y cells.

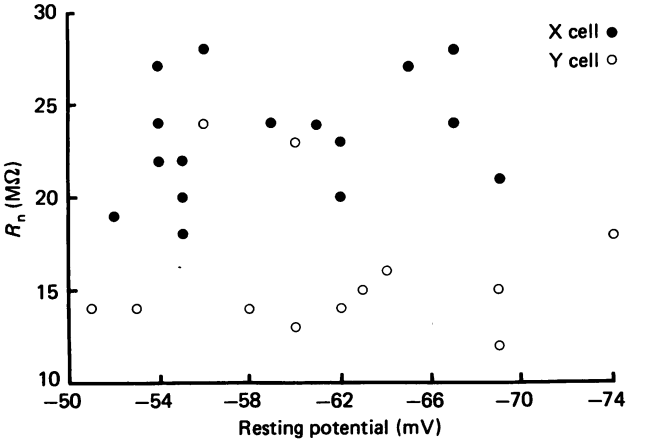

Fig. 14. Scatter plot of input resistance (R_n) and resting membrane potential for geniculate X and Y cells.

Fig. 15 illustrates the relationship between R_n and A_n as described by eqn. (7). The series of dashed curves represent lines of equal R_m for the varying values of L_n. The L_n values represented in the Figure are consistent with those derived in the present study for geniculate X and Y cells. The triangles represent the eight neurones described above that had their cable properties measured and were also labelled with HRP. Fig. 15 shows the slightly larger R_m values exhibited by X cells than by Y cells. More striking, however, is the tremendous range of R_m values indicated for X cells, whereas these values for Y cells fall within a narrow band of specific membrane iso-resistance lines. Given the assumption of a constant C_m across cells and the relationship described by eqn. (8), the results of Fig. 15 are consistent with the wider range of τ_m values displayed by X cells than by Y cells.

Because of the relatively small range of R_m values for Y cells, variations in R_n within this class show a simple relationship with cell size (see Fig. 15). This would be expected if changes in cell size reflected simple scaling rather than a change in the basic geometry of the dendritic tree. This conclusion is supported by the morphological relationships illustrated in Fig. 6. The variation in R_n of X cells, on the other hand, shows no simple relationship to either cell size or R_m. This suggests that

variations in the size of X cells may be associated with structural changes in dendritic geometry that will influence R_n values. As noted above, X cells exhibited greater variation than did Y cells both in the relationship between primary dendritic diameters and dendritic branching patterns (Fig. 6) as well as in the values of τ_1 (Fig. 9*C*). Both observations suggest a greater degree of structural heterogeneity in X cell arbors than in those of Y cells.

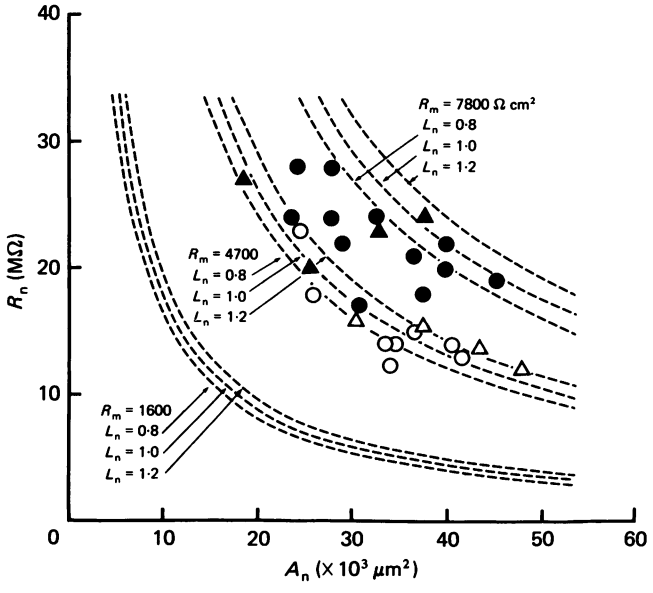

Fig. 15. Relationship between the total membrane surface area (A_n) and input resistance (R_n) of geniculate neurones. The dashed lines represent families of curves described by eqn. (11) for selected values of electrotonic length (L_n) and constant specific membrane resistance (R_m). The data include X and Y cells whose values for A_n were either measured histologically or estimated from electrical parameters (see text). ▲, X cells with morphologically determined A_n; ●, X cells with A_n estimated from biophysical parameters; △, Y cells with morphologically determined A_n; ○, Y cells with A_n estimated from biophysical parameters.

Relationships with membrane time constant (τ_m). There is no relationship between τ_m and cell size among our sample of geniculate X and Y cells (Fig. 16*A*). In contrast, we did find a significant correlation between τ_m and neuronal R_n for our entire population of geniculate X and Y cells (Fig. 16*B*; $r = +0{\cdot}65$; $P < 0{\cdot}001$). However, this seems to be an epiphenomenon of the above-mentioned fact that Y cells tend to have smaller values of both variables than do X cells, because no significant correlation exists between these parameters when X or Y cells are considered alone (for X cells, $r = +0{\cdot}21$ and $P > 0{\cdot}1$; for Y cells, $r = +0{\cdot}40$ and $P > 0{\cdot}1$). This latter conclusion is consistent with our observation of no clear correlation between R_n and R_m. Finally, the membrane time constant of geniculate cells bore no relationship with the resting membrane potential (Fig. 16*C*; for all cells, $r = -0{\cdot}28$; for X cells, $r = -0{\cdot}16$; for Y cells, $r = -0{\cdot}26$; $P > 0{\cdot}1$ for all correlations).

Relationships with electrotonic length. The whole neurone (L_n) and dendritic electrotonic lengths (L) of X and Y cells bore a strong linear relationship with each

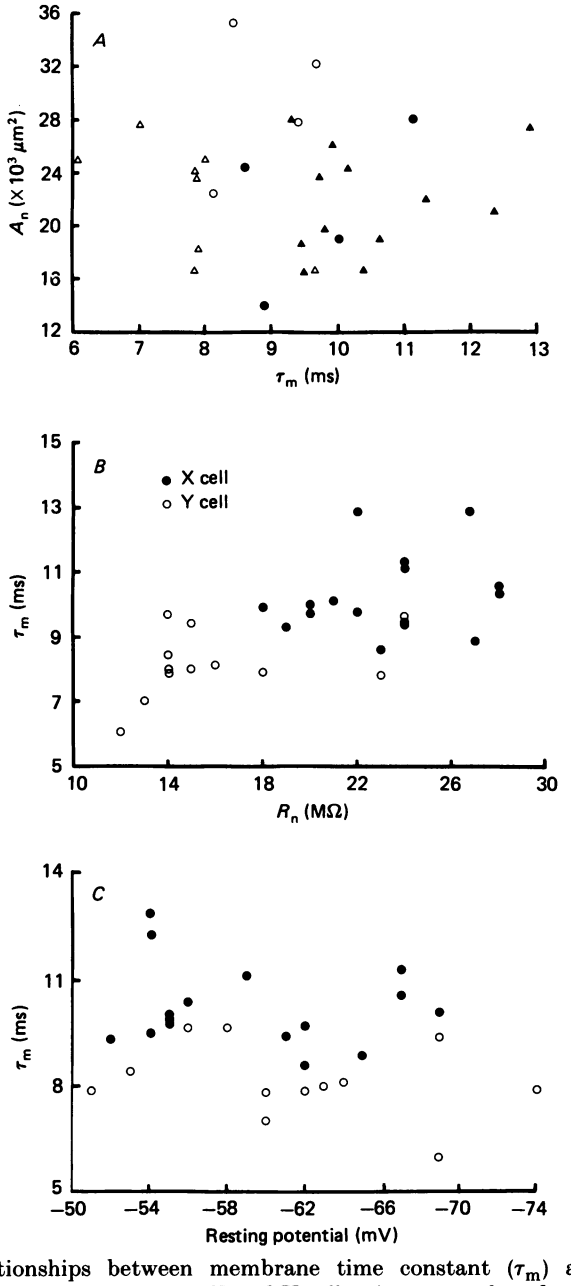

Fig. 16. Relationships between membrane time constant (τ_m) and various other electrical parameters of geniculate X and Y cells. *A*, scatter plot of relationship between the membrane surface area (A_n) and τ_m for twenty-eight geniculate X and Y cells. These data include cells whose values for A_n were either measured morphologically or estimated from electrical data. Symbols: ●, X cells with A_n measured morphologically; ▲, X cells with A_n estimated from electrical data; ○, Y cells with A_n measured morphologically; △, Y cells with A_n estimated from electrical data. *B*, scatter plot of the relationship between the input resistance (R_n) and τ_m of geniculate X and Y cells. Key in *B* applies to *C* as well. *C*, scatter plot of the relationship between the resting membrane potential and τ_m of geniculate X and Y cells.

other ($r > +0{\cdot}99$; $P < 0{\cdot}001$). Consequently, all relationships described for L can be applied to L_n as well.

A cell's electrotonic length depends largely on dendritic geometry and R_m, particularly since the equivalent cylinder model assumes constant internal and external resistance. Jack, Miller, Porter & Redman (1971) and Gustafsson & Pinter (1984) have shown that L is inversely proportional to the square root of τ_m (or R_m) as follows:

$$L \alpha (l/\sqrt{d})(\tau_m)^{-\frac{1}{2}}, \tag{12}$$

where l and d represent the length and diameter of the cylinder equivalent to the dendritic arbor. This inverse trend between τ_m and L exists for Y cells but not for

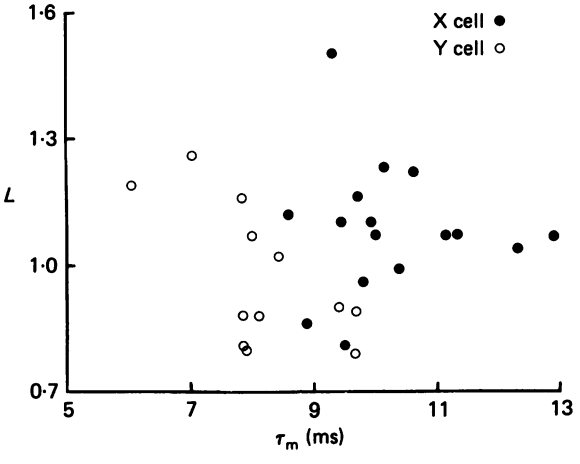

Fig. 17. Relationship between the electrotonic length (L) and membrane time constant (τ_m) of geniculate X and Y cells.

X cells (Fig. 17). There is no significant correlation between these parameters for our entire population of neurones ($r = +0{\cdot}05$; $P > 0{\cdot}1$) or for the X cells ($r = -0{\cdot}03$; $P > 0{\cdot}1$), but a significant correlation exists for Y cells ($r = -0{\cdot}66$; $P < 0{\cdot}01$). This relationship suggests that Y cells differ only in size (i.e. they are scaled versions of one another, since $l/\sqrt{d}$ remains fairly constant), and that L depends mostly on τ_m and thus on R_m. In contrast, X cells appear to have far greater heterogeneity in their dendritic geometry ($l/\sqrt{d}$ of the equivalent cylinder) and exhibit no obvious relationship between L and τ_m (or R_m). Together, these data provide yet further evidence, based totally on electrical measurements, that X cells are morphologically more diverse than are Y cells.

DISCUSSION

We measured the passive electrical properties of neurones from an *in vivo* preparation of the cat's lateral geniculate nucleus. These cable properties can be related to the wealth of morphological and physiological data already available for these neurones, including their classification as X and Y cells. In the following

sections, we discuss some implications of these findings as well as certain qualifications necessitated by technical considerations.

Morphometry

Technical considerations. Our morphological measurements were subject to errors introduced from two sources. First, most observations were made with the light microscope, which limits the resolution of measurements under ideal conditions to 0·2–0·3 μm. Our use of thick sections (100 μm) and white light reduces the useful resolution from this ideal limit, and we estimate our measurement resolution with the light microscope to be roughly 0·5 μm. Although this limit was not a significant problem for the measurements of soma diameters and the calibre of the relatively large proximal dendrites, the diameters of peripheral processes can approach 0·5 μm. We thus employed electron microscopy for determination of many diameters below 1·0 μm, but this cannot eliminate all error in our measurements.

A second source of error was tissue shrinkage resulting from histological processing. As described in Methods, we adjusted all of our measurements for an average shrinkage of 20%. However, we found some variation in tissue shrinkage not only between animals but occasionally between sections of tissue obtained from the same animal. Many of our labelled geniculate neurones were obtained from experiments in which an independent assessment of tissue shrinkage was not obtained, because we were not yet aware of the problem. Consequently, our use of an average 20% adjustment for all morphological measurements reduces but does not eliminate errors due to differential tissue shrinkage.

Dendritic branching. An important conclusion from our data is that geniculate X and Y cells obey the '$\frac{3}{2}$ power rule', thereby meeting one geometric precondition for modelling their dendritic arbors as equivalent cylinders. Although our measurements of dendritic diameters indicate some scatter for this constraint, this scatter bore no relationship to the diameter or location (i.e. distal *versus* proximal) of branch points and thus may simply reflect the above-mentioned errors inherent in our measures. In any case, the scatter in the relationship was not sufficient to obscure its obvious presence.

The $\frac{3}{2}$ power rule has been sought for many other neuronal types at a variety of loci with variable and often controversial results. Some studies of α-motoneurones of the spinal cord have argued that these neurones obey the $\frac{3}{2}$ power rule (Lux, Schubert & Kreutzberg, 1970; Brown & Fyffe, 1981; Ulfhake & Kellerth, 1981), while others deny this (Barrett & Crill, 1974; Egger & Egger, 1982). Brain-stem respiratory neurones (Kreuter, Richter, Camerer & Senekowitsch, 1977), retinal ganglion cells (Koch, Poggio & Torre, 1982), neocortical pyramidal cells (Hillman, 1979), and cerebellar Purkinje cells (Hillman, 1979) all fail to satisfy the $\frac{3}{2}$ power rule, whereas CA1 pyramidal cells (Turner & Schwartzkroin, 1980), hippocampal granule cells (Durand *et al.* 1983) and spinocervical tract neurones (Sedivec, Capowski & Mendell, 1985) follow this relationship. Curiously, those dentate granule cells located in the distal portions of the molecular layer obey the $\frac{3}{2}$ power relationship, while granule cells located elsewhere do not (Desmond & Levy, 1984).

Since many neuronal cell types in the mammalian central nervous system need not obey the $\frac{3}{2}$ power rule, one might ask what its functional significance is and why

geniculate X and Y cells in the cat represent cell types that adhere faithfully to this rule. It is certainly not present just to satisfy the needs of experimental models. Unfortunately, other than Rall's (1959*a*) original description of the $\frac{3}{2}$ power rule and subsequent references to it, we have found little in the literature that addresses the functional significance of this constraint (but see Rall, 1964).

Two general possibilities can be considered regarding the significance of the $\frac{3}{2}$ power rule. First, this branching pattern may simply reflect the structural or hydraulic needs of the dendritic arbor. That is, such a branching pattern may be an epiphenomenon of growth, or it may reflect the most efficient structure for the internal transport of various substances. While such explanations that do not relate primarily to neurone electrotonus cannot be ruled out, they seem unlikely or limited because so many neurones do not exhibit such a pattern of branching. Secondly, this branching pattern may represent an important means of controlling electrotonic signal transmission within a dendritic arbor. C. Koch (personal communication) has recently used computer simulations to model cells that follow the $\frac{3}{2}$ power rule. His results indicate that branch points satisfying this relationship exhibit the least attenuation of electrotonic conduction in *both* directions, and that any other branching pattern can maximize such conduction in only one direction. That is, dendritic branching patterns that obey the $\frac{3}{2}$ power rule not only permit efficient electrotonic conduction of post-synaptic potentials towards the soma, but they also permit efficient conduction towards the distal dendrites of currents generated at the soma and proximal dendrities. As a result, action potentials initiated in the soma or axon hillock, as well as synaptic potentials generated proximally, can invade the more distal dendrites and influence the further generation of synaptic potentials there. In this manner, the state of activity of a cell can regulate synaptic activation. Perhaps only certain cell types (such as geniculate X and Y cells) are designed with such a state-dependent gating of synaptic inputs in mind, whereas other neurones are designed to maintain constant post-synaptic potentials regardless of the cells' levels of activity.

Membrane surface area. A second interesting morphometric finding was the linear relationship between the diameter of the primary dendrite and the membrane surface area of the arbor emanating from that dendrite. The algorithm generated from this provides a relatively simple and straightforward method for calculating A_n without the tedious microscopic measurements previously required. Although we can offer no obvious functional explanation for such a relationship, either structural or electrical, it is interesting that analogous relationships have been previously reported for α-motoneurones (Ulfhake & Kellerth, 1981), γ-motoneurones (Ulfhake & Cullheim, 1981), and spinocervical tract neurones (Sedivec *et al.* 1985). However, the specific algorithm differs for each cell type, which apparently reflects differences in their sizes and in the geometry of their dendritic arbors.

Appropriateness of the equivalent cylinder model

As noted in Results, the equivalent cylinder model of neurones requires a number of assumptions, many of which are presently not amenable to experimental verification. In particular, we cannot evaluate the assumptions of somatic membrane isopotentiality or of uniform and negligible resistance in the internal and external

media. We can, however, address the other assumptions. One discussed immediately above that seems valid is the $\frac{3}{2}$ power rule. We also have shown that geniculate neurones respond in a passive manner under our experimental conditions and that terminal dendritic branches of a given cell end at roughly equal electrotonic distances.

Uniform specific membrane resistance (R_m). Another assumption of the equivalent cylinder model is that the neuronal membranes exhibit a uniform R_m. Although we did not examine this constraint directly, several points warrant discussion. Studies of spinal motoneurones (Barrett & Crill, 1974; Iansek & Redman, 1973; Fleshman, Segev, Cullheim & Burke, 1983) and hippocampal cells (Durand *et al.* 1983) suggest that R_m may be spatially non-uniform, with resistance increasing with distance from the soma. Barrett & Crill (1974) and Rall (1982) suggested that such non-uniformity of R_m would result in gross over-estimates of C_m since, as determined from somatic recordings, estimates of R_m would be low (see eqn. (8)).

Indeed, a number of studies of other neurone types utilizing techniques similar to those used here have produced C_m values that are much higher than the generally accepted value of 1·0 μF/cm^2 for biological membranes (Cole, 1968). The C_m values have been reported to be from 2·1 to 5·2 μF/cm^2 for spinal motoneurones (Barrett & Crill, 1974; Ulfhake & Kellerth, 1984), hippocampal granule cells (Durand *et al.* 1983), and hippocampal pyramidal cells (Turner & Schwartzkroin, 1980). Our derived value for C_m of 1·86 μF/cm^2 was also greater than the accepted value 1·0 μF/cm^2, although to a lesser degree than these other studies. While the C_m for geniculate neuronal membranes may be greater than 1·0 μF/cm^2, it seems reasonable to conclude that our derived values of R_m are underestimates for reasons such as ohmic shunting of the soma due to injury associated with the electrode penetration (Durand *et al.* 1983; Gustafsson & Pinter, 1984) and/or a non-uniform R_m.

Another significant factor that can lower the measured R_m from its true value is the conductance increase due to synaptic activation. In many neurones, including geniculate X and Y cells (Wilson *et al.* 1984), inhibitory synapses, which create relatively large increases in post-synaptic membrane conductance (Ben-Ari, Krnjevic, Reiffenstein & Reinhardt, 1981), tend to concentrate more on proximal than on distal dendritic locations. Thus any maintained level of afferent synaptic activity throughout a neurone's dendritic arbor is likely to increase ionic conductances (with an associated decrease in effective R_m) and should do so to a greater degree for proximal than for distal dendritic locations.

Unfortunately, it is not practical with an *in vivo* preparation such as ours to measure the effect of synaptic activity on R_m, since it is impossible for us to regulate this activity. Under our recording conditions, the X and Y cells are almost certainly under constant synaptic bombardment that will increase membrane conductance in a non-uniform manner throughout the dendritic arbor. It thus seems plausible that our derived values of R_m are artifactually low. This must remain an important caveat to our conclusions based on our derived cable properties of geniculate X and Y cells.

Distribution of synaptic inputs. The equivalent cylinder model allows representation of current injection to dendrites only if the current is injected at dendritic sites that are of equal electrotonic distance from the soma. Although this constraint may seem to reflect some ideal case, recent electron microscopic observations for geniculate neurones indicate that such a synaptic distribution indeed exists. Wilson *et al.* (1984)

showed that each population of synaptic input to geniculate X and Y cells, deriving from either retinal, cortical, or inhibitory terminals, innervate each neurone in a particular dendritic zone; these zones lie at different distances from the soma. More recently. Hamos *et al.* (1986) have shown that there is a direct correlation between actual length and electrotonic length of the dendrites of these cells. Taken together, these results suggest that each class of input terminates on different dendrites at a roughly constant electrotonic distance from the soma, but this constant distance differs among the afferent types. Consistent with this idea, Hamos *et al.* 1986 also showed that an individual retinal axon can contact each of its post-synaptic targets in a given geniculate cell at a fixed electrotonic distance from the soma.

Of course, current flow within the dendritic tree will also be affected by factors such as interactions among the synaptic inputs, voltage-dependent conductances, or membrane specializations such as spines that are not considered in the model (Dodge, 1979; Koch, 1985). However, the electrical parameters that we have derived for geniculate neurones using the equivalent cylinder model may be considered reasonable first approximations which will need to be modified as more physiological and anatomical information is provided for these cells. Indeed, the present data indicate that geniculate neurones meet many of the constraints posed by the equivalent cylinder model extraordinarily well.

Comparison with other neurones

The cable properties of geniculate X and Y cells derived in the present study are comparable to those of other neuronal types reported in other studies. The range of R_n values for geniculate cells (12–28 MΩ) was higher than the range of 0·5–4·0 MΩ reported for spinal motoneurones (Barrett & Crill, 1974; Burke *et al.* 1982; Ulfhake & Kellerth, 1984), but it is less than the range of 39–60 MΩ reported for hippocampal pyramidal cells (Brown *et al.* 1981*a*), granule cells (Brown *et al.* 1981*a*; Durand *et al.* 1983), and dorsal root ganglion cells (Brown *et al.* 1981*b*).

Our sample of geniculate neurones exhibited τ_m values that ranged from 6·04 to 12·89 ms. This compares to values of 11–19 ms reported for hippocampal pyramidal cells (Brown *et al.* 1981*a*) and hippocampal granule cells (Brown *et al.* 1981*a*) plus 3–9 ms for spinal motoneurones (Burke & ten Bruggencate, 1971; Ulfhake & Kellerth, 1984) and dorsal root ganglion cells (Brown *et al.* 1981*b*). Geniculate X and Y cells thus seem to possess τ_m values that fall within the reported range of these values for other neuronal types. As a result, the temporal summation properties of geniculate neurones appear to be somewhat intermediate among those of other cells in the central nervous system. Given the relationship defined by eqn. (8), a perusal of the literature shows that our estimates for R_m for these geniculate cells are comparable to such values for other neuronal types.

Finally, most neuronal types studied to date, including our sample of geniculate neurones, exhibit remarkably short electrotonic lengths of 0·9–1·8. These measures have been made for spinal motoneurones (Nelson & Lux, 1970; Lux *et al.* 1970; Jack *et al.* 1971; Burke & ten Bruggencate, 1971; Barrett & Crill, 1974; Ulfhake & Kellerth, 1984), hippocampal pyramidal and granule cells (Johnson, 1981; Brown *et al.* 1981*a*; Durand *et al.* 1983), red nucleus neurones (Tsukahara, Murakami & Hultborn, 1975),

and dorsal root ganglion cells (Brown *et al.* 1981*b*). These data indicate that, despite the immense heterogeneity seen in dendritic geometry for neurones of the central nervous system, most or all of these neurones maintain remarkably short electrotonic lengths, L. This property enables synaptic inputs throughout the dendritic arbor of a cell to influence responses at the soma and axon hillock. A conclusion of relatively small values for L almost seems tautological, since it seems implausible that neurones would grow such large dendritic arbors that many of their distally located synaptic inputs are electrically too distant from the soma to be functionally relevant.

However, it should be realized that the evidence for small L values applies only to Golgi type I cells (i.e. projection neurones), whose axons represent the sole output of these cells. This may not apply to Golgi type II cells (i.e. interneurones). Recent studies of amacrine cells of the vertebrate retina, which are interneurones with both presynaptic and post-synaptic contacts on their dendrites, indicate that these dendrites cover several electrotonic lengths (Ellias & Stevens, 1980; Miller & Bloomfield, 1983). Consequently, synaptic potentials may be effectively isolated from the soma and neighbouring branches, suggesting that individual dendrites constitute functional subunits. A morphological study of an interneurone of the cat's lateral geniculate nucleus also suggests such isolation of many of the cell's synaptic inputs (Hamos, Van Horn, Raczkowski, Uhlrich & Sherman, 1985).

Comparison of X and Y cell electrotonus

X and Y cells clearly differ in several of their passive cable properties, although these differences are not large in absolute terms. By examining the relationships between these parameters and neuronal morphology, we can determine which cable properties are likely to reflect size differences between X and Y cells and which require more sophisticated explanations.

Membrane time constant (τ_m) *and specific membrane resistance* (R_m). We assume that X and Y cells do not differ in terms of C_m, and our limited derivations of C_m support this assertion. Thus differences between X and Y cells in terms of their average τ_m values simply reflect differences in R_m. R_m (and thus τ_m) values were both higher and more variable for X than for Y cells. We cannot as yet determine whether this reflects an intrinsic difference between X and Y cells in terms of the make-up of their neuronal membranes or a difference in their synaptic inputs, which, as noted above, can alter ionic conductances and thus the observed values of R_m.

Indeed, differences between the pattern of synaptic inputs to X and Y cells may account for differences in their values of R_m. Nearly all synaptic inputs to Y cells terminate on dendritic shafts, whereas many retinal and inhibitory inputs to X cells terminate on dendritic appendages or spines (Wilson *et al.* 1984). Koch (1985) has demonstrated through computer modelling that the synaptic conductance changes for many of these inputs to X cell spines will be relatively isolated from the soma, whereas active synapses on Y cells will strongly influence the soma. Our recording electrodes inside somata would thus measure cable properties that might be less influenced by synaptic activity in X cells than in Y cells, with the result being that the observed R_m values would be higher for X cells than for Y cells.

We were struck by the considerable variability in R_m values of X cells. One simple explanation for this finding is that X cells exhibit heterogeneity in their intrinsic

membrane structure; this, in turn, may be related to the variability in X cell dendritic morphology (Friedlander *et al.* 1981; Weller & Humphrey, 1985). However, an alternative explanation is that the on-going synaptic activation of X cells, which will reduce membrane resistivity, is variable among individual cells. Several pieces of evidence support this latter contention. First, recent examinations of the micro-circuitry of geniculate neurones have shown that X cells vary considerably in the amounts of inhibitory innervation they receive (Wilson *et al.* 1984; Hamos *et al.* 1986). Secondly, geniculate X cells have recently been subtyped as 'normal' and 'lagged' (Mastronarde, 1983; Humphrey & Weller, 1985). The distinguishing feature of these subtypes is the powerful, short-latency inhibition seen in lagged X cell responses. In addition, X cells have been described with intermediate amounts of inhibition. Thus, both physiological and morphological evidence suggest that X cells receive inhibitory innervation of great variability, and this could result in the variable R_m values we have measured. Although it is possible to explain much of the difference in τ_m and R_m observed between geniculate X and Y cells without invoking intrinsic membrane differences, this does not rule out their existence. Regardless of their aetiology, these differences in observed R_m (and τ_m) represent important functional differences between X and Y cells that affect how these neurones integrate synaptic information.

Electrotonic length. The short electrotonic lengths of about 1·0 for both X and Y cells indicate that these geniculate neurones are electrically compact. One can appreciate this compactness by calculating the voltage attenuation factor (H) for a uniform cylinder of electrotonic length L from the formula (Jack *et al.* 1975):

$$H = V_0/V_L = \cosh(L), \tag{13}$$

where V_0 is the potential at the site of current injection, and V_L is the potential at the opposite end of the equivalent cylinder. Using our derived average values of L for geniculate cells, we calculate a value for H of 1·65 for X cells and 1·51 for Y cells. In terms of voltage attenuation seen at the soma, these values indicate that synaptic potentials generated at the most distal dendritic sites will decay by only 34% in Y cells and by 39% in X cells. Therefore, even the most distal excitatory synaptic innervation, thought to arise from visual cortex (Jones & Powell, 1969; Guillery, 1969*a*, *b*; Szentagothai, 1973; Wilson *et al.* 1984) is likely to have considerable influence on a neurone's somatic and axonal responses.

Can cable properties be used to distinguish X from Y cells? Although a major goal of the present study was to characterize the cable properties of geniculate X and Y cells and to correlate these with other morphological and physiological properties of these cells, we also wished to determine if these cable parameters can be used as criteria to identify these neurones as X or Y cells. Such an additional set of identifying criteria may represent the best or perhaps only means of identifying these cell classes under certain experimental conditions, such as *in vitro* preparations of the cat's lateral geniculate nucleus.

We explored this possibility in the following manner. For each cable parameter, the value that was half-way between the average value for all X cells and the average value for all Y cells was arbitrarily chosen as a cut-off point. For each cell, individual

values of electrical parameters were then assigned as X-like or Y-like depending on which side of the cut-off point they fell. This was then compared to the X–Y classification of the cell based on its receptive field properties and response latency to optic chiasm stimulation. In this manner, we examined the possibility of using individual values of R_n, τ_m, L and ρ to identify the functional class of a geniculate neurone. The accuracy rates for individual parameters were 89 % for R_n, 82 % for τ_m, 79 % for L, and 68 % for ρ. By combining the results for the first three parameters, we could predict the functional class of each of the twenty-eight geniculate cells with an accuracy of 93 %. Thus, at least in the *in vivo* preparation, cable properties can be regarded as useful criteria to identify geniculate neurones as X or Y cells. This reinforces the validity and appropriateness of identifying geniculate cells within the X–Y classification scheme.

Functional considerations. The clear differences in many of the membrane properties between X and Y cells indicate that these parameters vary as a consequence of physiological class and hence may be related to their unique functional roles. Furthermore, many of these differences were unrelated to morphological size, since these differences were present in those X and Y cells that exhibited overlap in their values of A_n. It is thus important to consider the influence that this difference in cable parameters between X and Y cells might have on their individual response properties.

Although many of the differences in membrane properties between X and Y cells were statistically significant, which serves to underscore the point that the X and Y cell pathways continue to be elaborated separately central to the retina, the functional relevance of these differences remains unclear in most cases. For example, the small difference in values of L between X and Y cells reflects only a 5 % difference in the attenuation of synaptic potentials as they travel from distal dendritic locations to the soma. In other words, a 20 mV post-synaptic potential generated at a distal dendritic site and recorded at the soma would differ by only 1 mV between X and Y cells. From a functional perspective, then, X and Y cells are much alike in terms of their electrical compactness.

The X cells exhibited higher τ_m values than did the Y cells. This will result in the generation of synaptic potentials in X cells that will last longer and permit increased temporal summation compared to the activity in Y cells. However, the extent to which this small difference of approximately 2 ms between the values of τ_m of X and Y cells will contribute to the difference in post-synaptic potentials and temporal response properties of these cells is unclear.

Finally, differences between X and Y cells with respect to R_n reflect the smaller A_n and slightly greater R_m values for X cells. The higher R_n values for X cells than for Y cells imply that, for equal amounts of synaptic current, the X cells would display somewhat larger synaptic potentials. It should be realized, however, that our values for R_n were measured with somatic recording and can thus differ significantly from the actual R_n at any specific synaptic site (cf. Koch & Poggio, 1983*b*). In addition, as pointed out by Koch & Poggio (1983*a*), synaptic activation can be thought of as producing a conductance change rather than an injection of current. As a result, synaptic sites with high input impedances can be very non-linear as they tend to saturate in potential, thereby limiting the inflowing current and consequently the potential change at the soma. Thus the validity of the generalization that the greater

R_n of X cells will result in greater amplification and efficacy of synaptic potentials than for Y cells will depend on the electrical and morphological features of individual synaptic sites.

Perhaps the most important difference we found was the higher R_m values of X cells than for the Y cells. Indeed, R_m (and τ_m) represents the only parameter in our study that is directly related to intrinsic membrane structure. Furthermore, differences in R_m between X and Y cells appear to be the basis for differences in their values for R_n and τ_m as well. As noted, it is not clear if these differences in R_m reflect differences in intrinsic membrane structure, differences in the pattern and activity of synaptic inputs, or other factors.

Whatever the cause of the R_m differences between X and Y cells, this still presents functional consequences. One consequence relates to the reduction of a neurone's L value as a function of its increased R_m. As noted above, X cells exhibit thinner dendrites than do Y cells. This would tend to produce relatively short space constants for X cells, thereby placing these cells at a disadvantage in terms of the propagation of synaptic potentials along the dendrites to the soma. The greater average R_m value of X cells than of Y cells will result in an increase in their dendritic space constants and, consequently, a reduction in their L values. Although X cells still display greater values of L than do Y cells, this difference in L would be correspondingly greater if X and Y cells exhibited equivalent R_m values.

In addition to R_m, the geometry of dendritic branching also has a major influence on values of L (eqn. (12)). However, although X cells show great heterogeneity in their dendritic geometry, they show rather constant values of L. We suggest that values for R_m may vary as a consequence of the branching pattern of X cells in order to maintain a constant and low value of L across these cells, values that are also comparable to those of the Y cells. This would explain the tremendous variability in R_m of X cells as reflecting the comparatively great heterogeneity of X cell dendritic geometry.

We wish to thank Dr Rosalyn Weller for participating in several of the experiments, Jin-Chang Cheng for computer programming, Joan Sommermeyer for excellent technical assistance, and Ellen Friedman for help with statistical analyses. We also thank Drs Wilfred Rall and Christof Koch for providing comments on the manuscript. This research was supported by USPHS Grants EY03038 and EY03604.

REFERENCES

ADAMS, J. C. (1977). Technical considerations on the use of horseradish peroxidase as a neuronal marker. *Neuroscience* **2**, 141–145.

AHLSÉN, G., LINDSTRÖM, S. & LO, F.-S. (1984). Inhibition from the brain stem of inhibitory interneurones of the cat's dorsal lateral geniculate nucleus. *Journal of Physiology* **347**, 593–609.

BARRETT, J. N. & CRILL, W. E. (1974). Specific membrane properties of cat motoneurones. *Journal of Physiology* **239**, 301–324.

BEN-ARI, Y., KRNJEVIC, K., REIFFENSTEIN, R. J. & REINHARDT, W. (1981). Inhibitory conductance changes and action of γ-aminobutyrate in rat hippocampus. *Neuroscience* **6**, 2445–2463.

BLOOMFIELD, S. A., HAMOS, J. E. & SHERMAN, S. E. (1985). Passive electrical properties of X- and Y-cells in the cat's lateral geniculate nucleus. *Neuroscience Abstracts* **11**, 232.

BLOOMFIELD, S. A. & SHERMAN, S. M. (1984). Morphometric and electrical properties of neurons in the lateral geniculate nucleus of the cat. *Neuroscience Abstracts* **10**, 56.

BROWN, A. G. & FYFFE, R. E. (1981). Direct observations on the contacts made between Ia afferent fibres and α-motoneurones in the cat's lumbosacral spinal cord. *Journal of Physiology* **313**, 121–140.

BROWN, T. H., FRICKE, R. A. & PERKEL, D. H. (1981*a*). Passive electrical constants in three classes of hippocampal neurones. *Journal of Neurophysiology* **46**, 812–827.

BROWN, T. H., PERKEL, D. H., NORRIS, J. C. & PEACOCK, J. H. (1981*b*). Electrotonic structure and specific membrane properties of mouse dorsal root ganglion cells. *Journal of Neurophysiology* **45**, 1–15.

BURKE, R. E., DUM, R. P., FLESHMAN, J. W., GLENN, L. L., LEV-TOV, A., O'DONOVAN, M. J. & PINTER, M. J. (1982). An HRP study of the relation between cell size and motor unit type in cat ankle extensor motoneurons. *Journal of Comparative Neurology* **209**, 17–28.

BURKE, R. E. & TEN BRUGGENCATE, G. (1971). Electrotonic characteristics of alpha motoneurones of varying size. *Journal of Physiology* **212**, 1–20.

CLELAND, B. G., DUBIN, M. W. & LEVICK, W. R. (1971). Sustained and transient neurones in the cat's retina and lateral geniculate nucleus. *Journal of Physiology* **217**, 473–496.

COLE, K. S. (1968). *Membranes, Ions and Impulses*. Berkeley: University of California Press.

CRICK, R. (1984). The function of the thalamic reticular complex: the searchlight hypothesis. *Proceeding of the National Academy of Sciences of the U.S.A.* **81**, 4586–4590.

DAVIS, L. & LORENTE DE NO, R. (1947). Contribution to the mathematical theory of electrotonics. *Studies of the Rockefeller Institute of Medical Research* **131**, 442–496.

DESCHENES, M., PARADIS, M., ROY, J. P. & STERIADE, M. (1984). Electrophysiology of neurons of lateral thalamic nuclei in cat: resting properties and burst discharges. *Journal of Neurophysiology* **51**, 1196–1219.

DESMOND, N. L. & LEVY, W. B. (1984). Dendritic caliber and 3/2 power relationship of dentate granule cells. *Journal of Comparative Neurology* **227**, 589–596.

DODGE, F. A. (1979). The nonuniform excitability of central neurons exemplified by a model of the spinal motoneuron. In *The Neurosciences Fourth Study Program*, ed. SCHMITT, F. O. & WORDEN, F. G., pp. 439–455. Cambridge, MA: M.I.T. Press.

DURAND, D., CARLEN, P. L., GUREVICH, N., HO, A. & KUNOV, H. (1983). Electrotonic parameters of rat dentate granule cells measured using short current pulses and HRP staining. *Journal of Neurophysiology* **50**, 1080–1097.

EGGER, M. D. & EGGER, L. D. (1982). Quantitative morphological analysis of spinal motoneurons. *Brain Research* **253**, 19–30.

ELLIAS, S. A. & STEVENS, J. K. (1980). The dendritic varicosity: a mechanism for electrically isolating the dendrites of cat retinal amacrine cell? *Brain Research* **196**, 365–372.

FERNALD, R. & CHASE, R. (1971). An improved method for plotting retinal landmarks and focusing the eyes. *Vision Research* **11**, 95–96.

FLESHMAN, J. W., SEGEV, I., CULLHEIM, S. & BURKE, R. E. (1983). Matching electrophysiological with morphological measurements in cat spinal α-motoneurone. *Neuroscience Abstracts* **46**, 341.

FOOTE, W. E., MORDES, J. P., COLBY, C. L. & HARRISON, T. A. (1977). Differential effect of midbrain stimulations on X-sustained and Y-transient neurons in the lateral geniculate nucleus of the cat. *Brain Research* **127**, 153–158.

FRIEDLANDER, M. J., LIN, C.-S., STANFORD, L. R. & SHERMAN, S. M. (1981). Morphology of functionally identified neurons in lateral geniculate nucleus of the cat. *Journal of Neurophysiology* **46**, 80–129.

GUILLERY, R. W. (1969*a*). The organization of synaptic interconnections in the laminae of the dorsal lateral geniculate nucleus of the cat. *Zeitschrift für Zellforschung und mikroskopische Anatomie* **96**, 1–38.

GUILLERY, R. W. (1969*b*). A quantitative study of synaptic interconnections in the dorsal lateral geniculate nucleus of the cat. *Journal of Comparative Neurology* **96**, 39–48.

GUSTAFSSON, B. & PINTER, M. J. (1984). Relations among passive electrical properties of lumbar α-motoneurones of the cat. *Journal of Physiology* **356**, 401–431.

HAMOS, J. E., VAN HORN, S. C., RACZKOWSKI, D. & SHERMAN, S. M. (1986). Synaptic circuits involving an individual retinogeniculate axon in the cat. *Journal of Comparative Neurology* (in the Press).

HAMOS, J. E., VAN HORN, S. G., RACZKOWSKI, D., ULHRICH, D. J. & SHERMAN, S. M. (1985). Synaptic connectivity of a local circuit neurone in lateral geniculate nucleus of the cat. *Nature* **317**, 618–621.

HILLMAN, D. E. (1979). Neuronal shape parameters and substructures as a basis of neuronal form. In *The Neurosciences: Fourth Study Program*, ed. SCHMITT, F. O. & WORDEN, F. G., pp. 477–498. Cambridge, MA: M.I.T. Press.

HOCHSTEIN, S. & SHAPLEY, R. M. (1976). Quantitative analysis of retinal ganglion cell classifications. *Journal of Physiology* **262**, 265–284.

HODGKIN, A. L. & RUSHTON, W. A. H. (1946). The electrical constants of a crustacean nerve fibre. *Proceedings of the Royal Society* B **133**, 444–479.

HOFFMANN, K.-P., STONE, J. & SHERMAN, S. M. (1972). Relay of receptive-field properties in dorsal lateral geniculate nucleus of the cat. *Journal of Neurophysiology* **35**, 518–531.

HUBEL, D. H. & WIESEL, T. N. (1961). Integrative action in the cat's lateral geniculate body. *Journal of Physiology* **155**, 385–398.

HUMPHREY, A. L., SUR, M., UHLRICH, D. J. & SHERMAN, S. M. (1985). Projection patterns of individual X- and Y-cell axons from the lateral geniculate nucleus to cortical area 17 in the cat. *Journal of Comparative Neurology* **233**, 159–189.

HUMPHREY, A. L. & WELLER, R. E. (1985). Functional subgroups among X-cells in the lateral geniculate nucleus of the cat. *Neuroscience Abstracts* **11**, 318.

IANSEK, R. & REDMAN, S. J. (1973). An analysis of the cable properties of spinal motoneurones using a brief intracellular current pulse. *Journal of Physiology* **234**, 613–636.

ITO, M. & OSHIMA, T. (1965). Electrical behaviour of the motoneurone membrane during intracellularly applied current steps. *Journal of Physiology* **180**, 607–635.

JACK, J. J. B., MILLER, S., PORTER, R. & REDMAN, S. J. (1971). The time course of minimal excitatory post-synaptic potentials evoked in spinal motoneurones by group Ia afferent fibres. *Journal of Physiology* **215**, 353–380.

JACK, J. J. B., NOBLE, D. G. & TSIEN, R. W. (1975). *Electrical Current Flow in Excitable Cells*, pp. 131–224. Oxford: Clarendon Press.

JACK, J. J. B. & REDMAN, S. J. (1971). An electrical description of the motoneurone, and its application to the analysis of synaptic potentials. *Journal of Physiology* **215**, 321–352.

JAHNSEN, H. & LLINÁS, R. (1984*a*). Electrophysiological properties of guinea-pig thalamic neurones: an *in vitro* study. *Journal of Physiology* **349**, 205–226.

JAHNSEN, H. & LLINÁS, R. (1984*b*). Ionic basis for the electroresponsiveness and oscillatory properties of guinea-pig thalamic neurones *in vitro*. *Journal of Physiology* **349**, 227–247.

JOHNSON, D. (1981). Passive cable properties of hippocampal CA3 pyramidal neurons. *Cellular Molecular Neurobiology* **1**, 41–55.

JONES, E. G. & POWELL, T. P. S. (1969). An electron microscopic study of the mode of termination cortico-thalamic fibers within the sensory relay nucleii of the thalamus. *Proceedings of the Royal Society* B **172**, 173–185.

KAPLAN, E. S., MARCUS, S. & SO, Y.-T. (1979). Effects of dark adaptation on spatial and temporal properties of receptive fields in cat lateral geniculate nucleus. *Journal of Physiology* **294**, 561–580.

KOCH, C. (1985). Understanding the intrinsic circuitry of the cat's LGN: electrical properties of the spine-triad arrangement. *Proceedings of the Royal Society* B **225**, 365–390.

KOCH, C. & POGGIO, T. (1983*a*). Electrical properties of dendritic spines. *Trends in Neurosciences* **6**, 80–83.

KOCH, C. & POGGIO, T. (1983*b*). A theoretical analysis of electrical properties of spines. *Proceedings of the Royal Society* B **218**, 455–477.

KOCH, C., POGGIO, T. & TORRE, V. (1982). Retinal ganglion cells: a functional interpretation of dendritic morphology. *Philosophical Transactions of the Royal Society B* **298**, 227–264.

KRAUTH, J. (1983). The interpretation of significance tests for independent and dependent samples. *Journal of Neuroscience Methods* **9**, 269–281.

KREUTER, F., RICHTER, D. W., CAMERER, H. & SENEKOWITSCH, R. (1977). Morphological and electrical description of medullary respiratory neurons of the cat. *Pflügers Archiv* **372**, 7–16.

LENNIE, P. (1980). Parallel visual pathways. *Vision Research* **20**, 561–594.

LUX, H. D., SCHUBERT, P. & KREUTZBERG, G. W. (1970). Direct matching of morphological and electrophysiological data in cat spinal motoneurones. In *Excitatory Synaptic Mechanisms*, ed. ANDERSEN, P. & JANSEN, J. K. S., pp. 189–198. Oslo: Universitets Forlaget.

MASTRONARDE, D. (1983). Subtypes of X relay cells in the cat LGN can be distinguished solely by responses to visual stimuli. *Investigative Ophthalmology and Visual Science* **24**, suppl., 265.

MENDENHALL, W. & SCHEAFFER, R. L. (1973). *Mathematical Statistics with Applications*, pp. 348–351. North Scituate: Duxbury Press.

MILLER, R. F. & BLOOMFIELD, S. A. (1983). Electroanatomy of a unique amacrine cell in the rabbit retina. *Proceedings of the National Academy of Sciences of the U.S.A.* **80**, 3069–3073.

NELSON, P. G. & LUX, H. D. (1970). Some electrical measurements of motoneuron parameters. *Biophysical Journal* **10**, 55–73.

RALL, W. (1959*a*). Branching dendritic trees and motoneuron membrane resistivity. *Experimental Neurology* **1**, 491–527.

RALL, W. (1959*b*). Dendritic current distribution and whole neuron properties. In *Research Report NM 01 05 00.01.02*, vol. 17, pp. 479–526. Bethesda: Naval Medical Research Institute.

RALL, W. (1964). Theoretical significance of dendritic trees for neuronal input–output relations. In *Neural Theory and Modeling*, ed. REIS, R., pp. 73–97. Stanford: Stanford University Press.

RALL, W. (1969). Time constants and electrotonic length of membrane cylinders and neurons. *Biophysical Journal* **9**, 1483–1508.

RALL, W. (1970). Cable properties of dendrites and effects of synaptic location. In *Excitatory Synaptic Mechanisms.*, ed. ANDERSON, P. & JANSEN, J. K. S., pp. 175–187. Oslo: Universitets Forlaget.

RALL, W. (1977). Core conductor theory and cable properties of neurons. In *Handbook of Physiology*, section 1; *The Nervous System*, vol. 1: *Cellular Biology of Neurons*, ed. KANDEL, E. R. & GEIGER, S., pp. 39–97. Bethesda: American Physiological Society.

RALL, W. (1982). Theoretical models which increase R_m with dendritic distance help fit lower values of C_m. *Neuroscience Abstracts* **8**, 414.

ROY, J. P., CLERCQ, M., STERIADE, M. & DESCHENES, M. (1984). Electrophysiology of neurons of lateral thalamic nuclei in cat: mechanisms of long-lasting hyperpolarizations. *Journal of Neurophysiology* **51**, 1220–1235.

SANDERSON, K. J. (1971). The projection of the visual field to the lateral geniculate and medial interlaminar nuclei in the cat. *Journal of Comparative Neurology* **143**, 101–118.

SANDERSON, K. J. & SHERMAN, S. M. (1971). Naso-temporal overlap in visual field projected to lateral geniculate nucleus in the cat. *Journal of Neurophysiology* **34**, 453–466.

SEDIVEC, M. J., CAPOWSKI, J. J. & MENDELL, L. M. (1985). Morphology of HRP-injected spino-cervical tract neurons: effect of dorsal rhizotomy. *Journal of Neuroscience* **6**, 661–672.

SHAPLEY, R. & LENNIE, P. (1985). Spatial frequency analysis in the visual system. *Annual Review of Neuroscience* **8**, 547–583.

SHERMAN, S. M. (1985). Functional organization of the W-, X- and Y-cell pathways in the cat: a review and hypothesis. In *Progress in Psychobiology and Physiological Psychology*, vol. 11, ed. SPRAGUE, J. M. & EPSTEIN, A. N., pp. 233–314. New York: Academic Press.

SHERMAN, S. M. & KOCH, C. (1986). The control of retinogeniculate transmission in the mammalian lateral geniculate nucleus. *Experimental Brain Research* **63**, 1–20.

SHERMAN, S. M. & SPEAR, P. D. (1982). Organization of visual pathways in normal and visually deprived cats. *Physiological Reviews* **62**, 738–855.

SINGER, W. (1973). The effect of mesencephalic reticular stimulation on intracellular potentials of cat lateral geniculate neurons. *Brain Research* **61**, 35–54.

SINGER, W. (1977). Control of thalamic transmission by corticofugal and ascending reticular pathways in the visual system. *Physiological Reviews* **57**, 386–420.

SO, Y.-T. & SHAPLEY, R. (1981). Spatial tuning of cells in and around lateral geniculate nucleus of the cat: X and Y relay cells and perigeniculate interneurons. *Journal of Neurophysiology* **45**, 107–120.

STANFORD, L. R., FRIEDLANDER, M. J. & SHERMAN, S. M. (1983). Morphological and physiological properties of geniculate W-cells of the cat: a comparison with X- and Y-cells. *Journal of Neurophysiology* **50**, 582–608.

STONE, J., DREHER, B. & LEVENTHAL, A. (1979). Hierarchical and parallel mechanisms in the organization of visual cortex. *Brain Research Reviews* **1**, 345–394.

SUR, M. & SHERMAN, S. M. (1982). Retinogeniculate terminations in cats: morphological differences between X- and Y-cell axons. *Science* **218**, 389–391.

SZENTÁGOTHAI, J. (1973). Neuronal and synaptic architecture of the lateral geniculate nucleus. In *Handbook of Sensory Physiology*, vol. VII/3, *Central Processing of Visual Information*, part B, *Visual Centers in the Brain*, ed. JUNG, R., pp. 141–176. Berlin: Springer-Verlag.

TSUKAHARA, N., MURAKAMI, F. & HULTBORN, H. (1975). Electrical constants of neurons of the red nucleus. *Experimental Brain Research* **23**, 49–64.

TURNER, D. A. & SCHWARTZKROIN, P. A. (1980). Steady-state electrotonic analysis of intracellularly-stained hippocampal neurons. *Journal of Neurophysiology* **44**, 184–199.

ULFHAKE, B. & CULLHEIM, S. (1981). A quantitative light microscopic study of the dendrites of cat spinal γ-motoneurons after intracellular staining with horseradish peroxidase. *Journal of Comparative Neurology* **202**, 585–596.

ULFHAKE, B. & KELLERTH, J.-O. (1981). A quantitative light microscopic study of the dendrites of cat spinal α-motoneurones after intracellular staining with horseradish peroxidase. *Journal of Comparative Neurology* **202**, 561–569.

ULFHAKE, B. & KELLERTH, J.-O. (1984). Electrophysiological and morphological measurements in cat gastrocnemius and soleus α-motoneurones. *Brain Research* **307**, 167–169.

WELLER, R. E. & HUMPHREY, A. L. (1985). Structural correlates of functional subgroups among X-cells in the cat LGN. *Neuroscience Abstracts* **11**, 318.

WILSON, J. R., FRIEDLANDER, M. J. & SHERMAN, S. M. (1984). Fine structural morphology of identified X- and Y-cells in the cat's lateral geniculate nucelus. *Proceedings of the Royal Society* B **221**, 411–436.

EXPLANATION OF PLATE

Photomicrographs of HRP-labelled geniculate neurones in 100 μm thick coronal sections. *A*, physiologically characterized X cell that was subsequently labelled with HRP. The arrow points to the portion of dendritic arbor that is shown in Fig. 2*A* and *B*. Calibration bar = 50 μm and applies to *B* as well. *B*, HRP-labelled geniculate Y cell. The arrow points to the portion of dendritic arbor that is shown in Fig. 2*C* and *D*. *C*, HRP-labelled geniculate X cell that was analysed biophysically and shown in Fig. 11. Calibration bar = 15 μm.

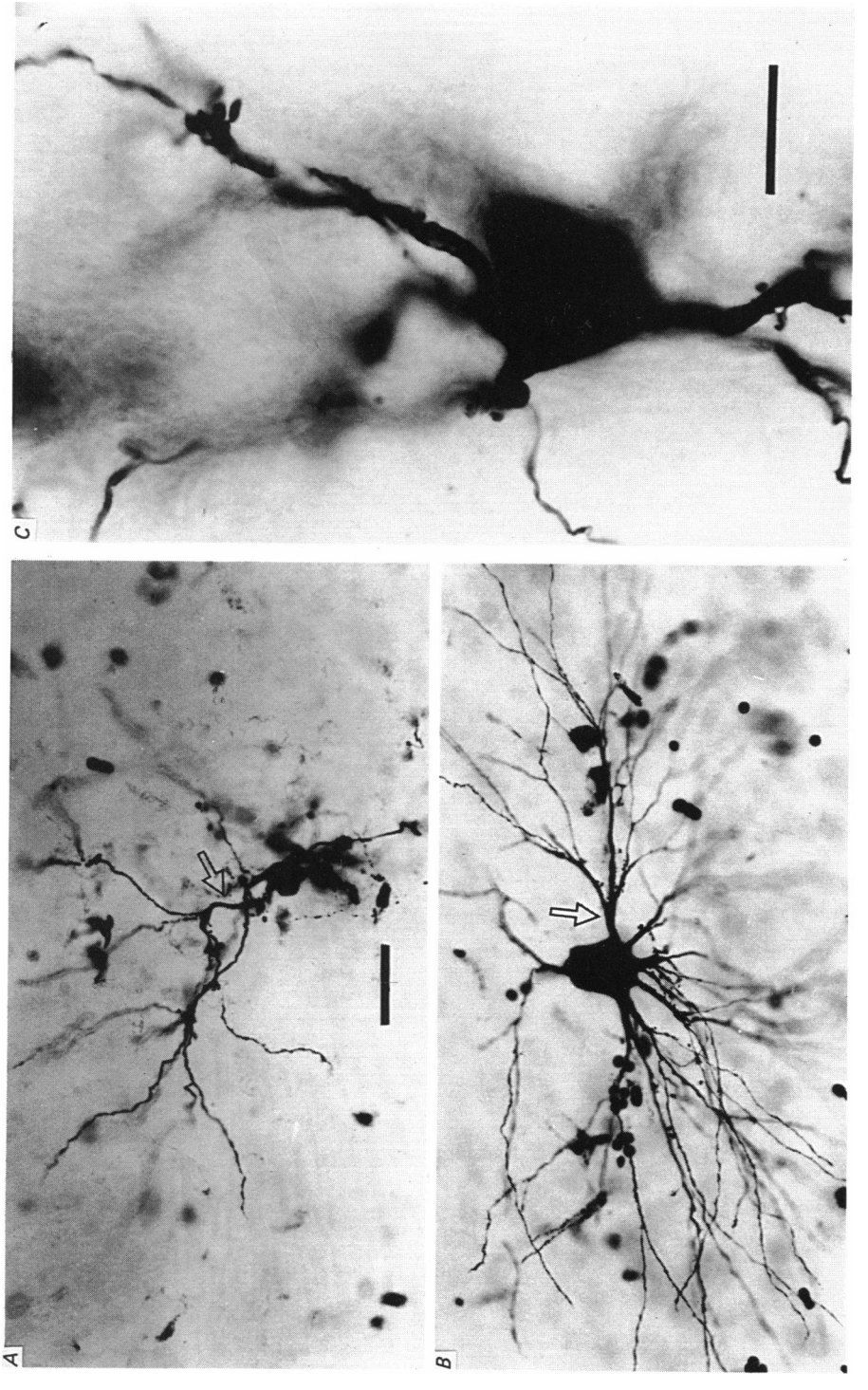
C
A
B